RUSSIAN JOURNAL OF EARTH SCIENCES, VOL. 3, NO. 1, PAGES 33–57, MARCH 2001

Volcanic and geodynamic evolution of the Bouvet triple junction: Evidence from basalt chemistry

A. A. Peyve and S. G. Skolotnev

Geological Institute (GIN), Russian Academy of Sciences

Abstract. This study focuses on mafic volcanic rocks from the Bouvet triple junction, which fall into six geochemically distinct groups: (1) N-MORB, the most widespread type, encountered throughout the study area. (2) Subalkaline volcanics, hawaiites and mugearites, strongly enriched in lithophile elements and radiogenic isotopes and composing the Bouvet volcanic rise, and compositionally similar basalts and basaltic andesites from the Spiess Ridge, generated in a deeper, fertile mantle region. (3) Relatively weakly enriched basalts, T-MORB, derived by the mixing of Type 1 and 2 melts and exposed near the axes of the Mid-Atlantic, Southwest Indian, and America-Antarctic ridges. (4) Basalts with a degree of trace lithophile element enrichment similar to the Spiess Ridge and Bouvet I. rocks, but higher in K, P, Ti, and Cr. These occur within extensional structures: the rift valley of the Southwest Indian Ridge, grabens of the East Dislocation Zone, and the linear rise between the Spiess Ridge and Bouvet volcano. Their parental melts presumably separated from a plume material that spread from the main channels and underwent fluid-involving differentiation in the mantle. (5) A volcanic suite ranging from basalt to rhyolite, characterized by low concentrations of lithophile elements, particularly TiO_2, and occurring on the Shona Seamount and other compressional features within the Antarctic and South American plates near the Bouvet triple junction. Unlike Types 1 to 4, which display tholeiitic differentiation trends, this suite is calc-alkaline. Its parental melts were presumably related to a plume material as well but, subsequently, they underwent a profound differentiation involving fluids and assimilated surrounding rocks in closed magma chambers in the upper mantle. Alternatively, the Shona Smt. might be a fragment of an ancient oceanic island arc. (6) Enriched basalts, distinguished from the other enriched rock types in having very high P and radiogenic isotope abundances and composing a tectonic uplift near the junction of the three rifts. It thus follows that the main factors responsible for the compositional diversity of volcanic rocks in this region include (i) mantle source heterogeneity, (ii) plume activity, (iii) an intricate geodynamic setup at the triple junction giving rise to stresses in adjacent plate areas, and (iv) the geological prehistory. The slow spreading rate and ensuing inefficient mixing of the heterogeneous mantle material result in strong spatial variations in basaltic compositions.

Paper number TJE01052.
CCC: 0000–0000/2001/0301–00052$18.00

The online version of this paper was published July 31, 2001.
URL: http://rjes.agu.org/v03/tje01052/tje01052.htm
Print companion will be issued.

Introduction

In the world ocean, there are only a few localities in which three tectonic plates meet at a point. These are, as a rule, complexly built regions integrating structural features of various types and exhibiting diverse magmatism. The latter reflects the parameters of magmatic systems and mantle composition beneath one or another mid-oceanic ridge.

The study of triple-junction magmatism offers a unique insight into the mantle geodynamics of interacting lithospheric plates during crust generation at mid-oceanic ridges. At the Bouvet triple junction (Bouvet TJ), the crust generation process is overprinted by plume magmatism. In this area an active volcanic rise, Bouvet I., is situated, which is viewed as an oceanic hot spot. Besides, just north of the Bouvet TJ, numerous seamounts and rises (Discovery, Shona, etc.) are located that are made up of basalts of non-rift affinity.

It is common knowledge that basalts, which are the most widespread rock type in the upper oceanic crust, bear information not only on their fractionation, seafloor eruption, and subsequent alteration processes, but also on the mantle composition and structure. The study of basalts sheds light on oceanic crust-forming processes and regional characteristics of basaltic magmatism, as well as the geodynamic environment in which the Bouvet TJ has evolved.

Bouvet TJ: Structural Setting and Previous Research

The Bouvet TJ, situated in the South Atlantic at ca. 55°S, is the point at which the South American, African, and Antarctic plates meet. The first study centered on the Bouvet TJ using echo sounding and magnetic measurements was carried out in 1974 [*Sclater et al.,* 1976]. Cruise 18 of the R/V Akademik Nikolaj Strakhov, in 1994, involved detailed structural studies of the Mid-Atlantic Ridge (MAR), northern Spiess Ridge, and Southwest Indian Ridge (SWIR) over the area between the Bouvet and Moshesh fracture zones [*Mazarovich et al.,* 1995; *Peyve et al.,* 1994, 1995]. In 1995, British researchers used sidescan sonar imaging to survey the neighborhood of the Bouvet TJ and Spiess Ridge [*Mitchell and Livermore,* 1998]. Further data were acquired by the R/V Gelendzhik in 1996 [*Carrara et al.,* 1997; *Ligi et al.,* 1997, 1999; Peyve et al., 1999]. The studies performed enabled the recognition of four morphologic provinces: (i) MAR structures, (ii) SWIR structures and the region of their junction with the MAR, (iii) America-Antarctic Ridge (AAR) structures and the region of their convergence with the MAR, and (iv) junction zone of the fossil structures pertaining to the MAR, SWIR, and AAR. We will also address volcanic chemistries from the Shona Smt. This is an equidimensional rise located 200 km west of the MAR axis at 54°30′, not belonging directly to the Bouvet TJ region, but of interest to unraveling the processes at work there (Figure 1).

The MAR structures are represented by three rift-valley segments between 53°20′ and 54°55′ S, with parallel ridges and depressions trending NNW-SSE. The southern rift valley segment bifurcates in two minor troughs: western, similar in trend to the AAR axis, and eastern, similar in trend to the SWIR axis. They are also loci of rift-related volcanism.

The crust generated at MAR displays rather regularly alternating magnetic lineations, which have been traced as far eastward as Chron C3Bn [*Ligi et al.,* 1999], corresponding roughly to 7 Ma [*Cande and Kent,* 1995].

SWIR structures and the region of their convergence with the MAR structures. In the study area, the Southwest Indian Ridge is represented by two segments offset by the Bouvet Fracture Zone. The axial part of the eastern segment has a strongly uplifted, shallow, asymmetrical rift valley. Its western flank is adjoined by the structures of the large tectono-volcanic Bouvet Rise, crowned by the Bouvet volcano. The western segment of the SWIR is the Spiess Ridge, as wide as 55 km and bounded by steep step-like slopes. The ridge's top surface lies in water depths of 1400 to 1700 m. In its central part a large volcanic edifice over 15 km in diameter rises, which is slightly elongated ESE, with a caldera 1 km by 2.5 km in size. The volcano's summit lies in water depths of 800–900 m. The Spiess Ridge is typified by numerous cone-shaped rises, evidently representing minor volcanoes. The ridge's axial part is noted for extremely strong magnetic anomalies, exceeding considerably those in the MAR rift valley and induced likely by recent volcanism. In the southwest part of the ridge, including its base, discernible is one more chron, C2n, whose trend matches that of the Spiess Ridge. This ridge can thus be assumed to be no older than 2 or 2.5 Ma.

Between the Spiess Ridge and Bouvet Rise, a number of rises extend obliquely to the SWIR structures. The largest of these *linear rises,* some 120 km long, commences south of the Bouvet FZ and extends as far as Bouvet I.

The convergence zone of the SWIR and MAR fossil structures is modified by the so-called *East Dislocation Area,* situated north of the Bouvet FZ valley, between the fracture zone and features that trend parallel to the MAR. This zone is represented by rises with steep slopes, often of an elongate triangular shape in plan view, separated by chains of depressions. These depressions are of a graben origin [*Ligi et al.,* 1999].

AAR structures and the region of their convergence with the MAR structures. In the study area, the largest structural feature of the AAR is the Conrad Fracture Zone, which is bordered on the north by the westernmost AAR segment. Within this segment, the AAR axis is expressed by a deep rift valley, which gives way northward to the Oblique Trough, a wide depression running aslant to the rift. The trough shows features of both sinistral shear and oblique spreading. Between the rift valley and the Conrad FZ, a large inner corner high is developed, which has a flattened top, and whose western part is surmounted by a conical edifice. On the opposite side of the rift, developed is an outer corner high, also crowned by a conical edifice. Beyond these rises, one finds structural features with AAR strikes, spread as far as the crustal areas with ages of ca. 6.5 to 7 Ma inclusive (magnetic Chron C3An) [*Ligi et al.,* 1999].

The area in which the MAR and AAR structures converge is complexly built. In the westernmost part of this area, the AAR rift mountains pass directly into the MAR rift mountains. Nearing the Oblique Trough, many structures of both the MAR and AAR become deformed, which is expressed in changes in their strike. According to *Skolotnev* [2000], such a pattern of the sea floor reflects a compressional regime during its formation.

The zone in which the MAR, SWIR, and AAR fossil structures converge is bounded on the south by passive seg-

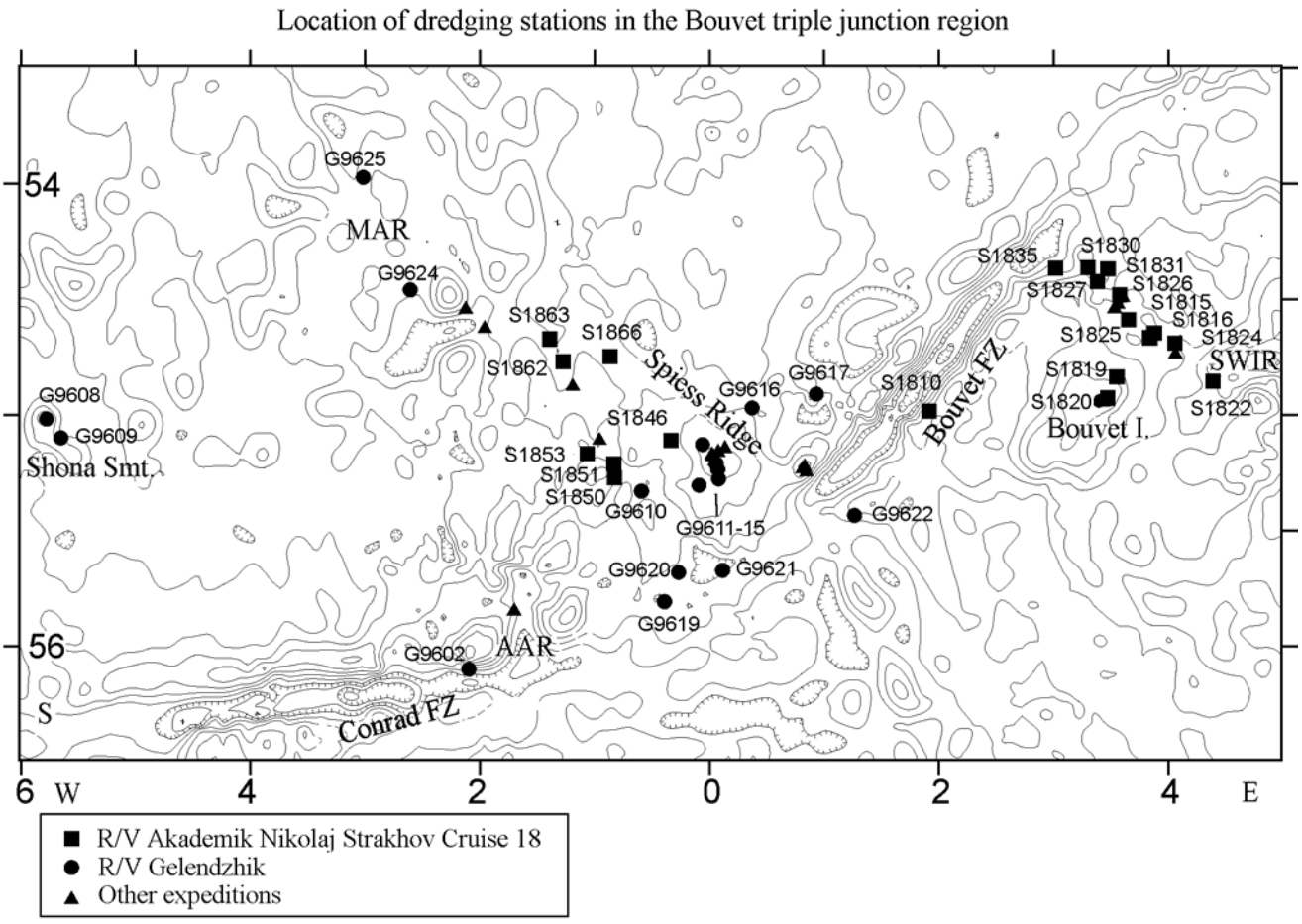

Figure 1. Location of dredging stations.

ments of the Conrad and Bouvet fracture zones and on the north by the two troughs forming the bifurcation of the southern MAR's tip. In the northern part of the zone, a rise is developed between these two troughs, modified by smaller-scale features with strikes characteristic of the MAR. In its southern part, structural features with AAR and SWIR strikes come into contact, showing over a stretch of 35 km offset relative to one another. This portion of the Antarctic plate is also characterized by a compressional regime [Skolotnev, 2000].

The Shona Seamount is situated at 54°32′ S, 5°50′ W. It consists of two rises, the main of which has a rounded shape with a leveled top surface. Its base is 9 km in diameter, with a minimum water depth over the top of 925 m b.s.l. East of this rise, two minor volcanic cones 1 km in diameter occur in water depths of 1500 m. Another rise is located further southeast in water depths of 1650 m. Its top part exhibits two craters less than 1 km in diameter and ca. 100 in depth. On the north, this rise is bounded by a tectonic scarp trending NW-SE.

Seafloor structure at the Bouvet TJ is thus very complex and displays numerous features atypical of crestal parts of mid-oceanic ridges developed both along divergent margins and within tectonic plates. This precludes an unequivocal interpretation for the geodynamic setting and geological evolution of this region.

Several models for the geological evolution of the Bouvet TJ have been put forward [*Apotria and Gray,* 1985, 1988; *Kleinrock and Morgan,* 1988; *Sclater et al.,* 1976]. Models accounting for the latest data are given in [*Ligi et al.,* 1999; *Peyve et al.,* 1999; *Skolotnev,* 2000]. These models show the steady development of the ridge-transform-transform junction, which had persisted for ca. 20 m.y., to have been upset at ca. 10 Ma. From that point in time on, the Bouvet TJ changed its configuration repeatedly, with stresses arising periodically over adjoining plate portions. The general sense of the Bouvet TJ development has consisted in the northward propagation of the SWIR and AAR, with the volcano-tectonic activity at MAR migrating in the same direction. At about 2 to 2.5 Ma, the development of the triple junction was complicated by mantle plume activity near the Spiess Ridge. The present-day Bouvet TJ configuration took shape at ca. 1 Ma and, in our opinion, the Bouvet TJ cannot be visualized as a single point but, rather, as a large area of interplay of various structural features through time and space [*Peyve et al.,* 1995].

Table 1. Coordinates of dredging stations that sampled basalts used in this study

Station	Latitude	Longitude
S1810	−54.48	1.91
S1815	−54.14	3.87
S1816	−54.17	3.83
S1819	−54.33	3.54
S1820	−54.43	3.46
S1822	−54.35	4.38
S1824	−54.19	4.05
S1825	−54.09	3.64
S1826	−53.98	3.57
S1827	−53.86	3.29
S1830	−53.87	3.46
S1831	−53.92	3.37
S1835	−53.87	3.01
S1846	−54.61	−0.34
S1850	−54.77	−0.84
S1851	−54.71	−0.84
S1853	−54.67	−1.07
S1862	−54.27	−1.28
S1863	−54.17	−1.40
S1866	−54.25	−0.87
G9602	−55.60	−2.11
G9608	−54.52	−5.79
G9609	−54.60	−5.66
G9610	−54.83	−0.60
G9611	−54.71	0.05
G9612	−54.74	0.06
G9613	−54.78	0.07
G9614	−54.80	−0.10
G9615	−54.63	−0.07
G9616	−54.47	0.36
G9617	−54.41	0.92
G9619	−55.31	−0.40
G9620	−55.18	−0.28
G9621	−55.17	0.11
G9622	−54.93	1.26
G9624	−53.96	−2.62
G9625	−53.47	−3.03

Notes: S18 – 18, R/V Akademik Nikolaj Strakhov cruise; G96, R/V Gelendzhik cruise.

Petrography, Mineralogy, and Spatial Distribution of Volcanic Rocks

Within the Southwest Indian Ridge, basalts and more silicic derivatives have been sampled from the rift valley southeast of the Bouvet Fracture Zone and its adjacent rift mountains, from the Bouvet FZ walls, and from the Spiess Ridge.

On the *Spiess Ridge,* samples were dredged from a caldera near the top of a large volcanic edifice (St. G9611, G9612) and from its lower slope (St. G9613), as well as from several smaller volcanoes (Figure 1, Table 1). Two of them lie on a line on both sides of the Spiess caldera (St. G9614 in the west and G9616 in the east) and possibly mark a fault. North of the caldera, in the axial part of the Spiess Ridge, a parasitic cone has been studied (St. G9615). The samples recovered are distinguished primarily by a strong predominance of vesicular varieties. Volcanics with ca. 10–15% vesicles, represented by pillow fragments, were sampled at St. G9615. More vesicular (20–50%) varieties make up flattened, intricately shaped pillows with several chilled zones and numerous large voids inside and fragments of the tops of pahoehoe lava flows. They exhibit distinct flow structures defined by a roughly parallel arrangement of elongated vesicles and are spread mainly near the caldera. The most vesicular (up to 80%) varieties are encountered as small, up to 8–10 cm across, angular fragments and represent volcanic scoria. On splitting, they give off a hydrogen sulfide odor.

The least vesicular (2–3%) basalts were dredged from the lower part of a major volcano (St. G9613). A clear dependency thus exists between the vesiculation of volcanites making up pillows and lava flows and their hypsometric position: the higher upslope the greater the vesiculation. The dredged volcanics are dominantly aphyric, and some contain a minor amount, as a rule, no greater than 1clinopyroxene phenocrysts. Microprobe measurements were made on sporadic grains of plagioclase (An_{66} from Sample G9614/27), clinopyroxene (Fs_{20} from G9612/30) and olivine (Fo_{86} from G9616/4) (Tables 2, 3, 4).

The groundmass in the volcanics is, as a rule, poorly crystalline and consists of small microlites of plagioclase An_{42-48} (Table 2), clinopyroxene, at times with a pinkish tint, and oxide phases. Strongly vesicular varieties making up scoria and the tops of lava flows commonly have a hyalopilitic groundmass with abundant extremely thin crystallites of an oxide phase immersed in a poorly crystalline matrix.

The alteration degree of Spiess Ridge volcanics depends to some extent on their structure and texture. The weakly and moderately vesicular varieties are fresh, with only a minor amount of glauconite (Table 5), partially filling in vesicles within dark-colored haloes developed along contraction joints in the pillows. The strongly vesicular varieties are often red-colored due to extensive precipitation of iron oxides and hydroxides. Some oxidized samples also exhibit a very peculiar newly formed finely dispersed phase, yellow in color, on the surface of some vesicles. This is a polymineralic aggregate composed of very fine (∼1 mcm), poorly crystalline grains, which obstructs the determination of their composition. Table 5 lists the most tenable microprobe determinations for these alteration products. They are closest in composition to clinopyroxene and orthoclase. Alteration products of similar aspect and composition have been described from recent on-land basalts as resulting from pneumatolytic metasomatism [*Skolotnev,* 1984].

Some very strongly altered volcanics are also encountered, whose alteration took place within thermal sites. Sample G9612/30 contains abundant palagonite after glass; G9612/29 and G9612/34, zeolite and barite aggregates; and in G9614/35, the glass is replaced by nontronite (Table 5). The structural and textural traits of the Spiess Ridge volcanics thus suggest that, as the ridge was in the making, the growth of the volcanic edifice involved submarine eruptions of pillow lava giving way to less viscous lavas, cooling into strongly vesicular volcanites in a highly oxidizing medium.

Table 2. Electron microprobe analyses of plagioclases

	1	2	3	4	5	6	7	8	9	10	11	12	13	14
	G9608/5	G9608/27	G9608/42	G9608/55	G9608/55	G9609/10	G9609/16	G9610/30	G9612/6	G9612/29	G9612/30	G9614/27	G9617/1	G9619/16
SiO_2	45.05	43.28	46.79	44.25	44.57	44.42	53.17	51.34	58.05	55.63	56.07	51.38	51.21	46.73
Al_2O_3	34.60	35.33	33.07	33.98	34.70	35.53	28.70	29.39	24.68	26.31	26.27	29.75	29.70	33.04
FeO	0.72	0.55	0.76	0.80	0.81	0.80	0.57	0.58	0.73	0.71	0.58	0.54	0.76	0.27
MgO	0.18	0.00	0.00	0.02	0.38	0.00	0.00	0.00	0.00	0.00	0.00	0.00	0.00	0.00
CaO	17.78	19.42	17.28	18.34	18.05	18.61	12.50	13.85	8.59	9.74	9.72	13.41	13.63	17.78
Na_2O	2.08	0.97	1.35	0.89	0.96	0.61	4.60	3.56	6.36	5.37	6.08	3.57	3.65	1.02
K_2O	0.04	0.03	0.14	0.00	0.06	0.00	0.27	0.24	0.32	0.25	0.21	0.23	0.25	0.04
Total	100.55	99.65	99.54	98.47	99.83	100.10	100.03	98.96	98.73	98.01	98.93	98.88	99.20	98.88
An	87	96	86	92	89	92	61	68	42	48	47	66	67	89
	15	16	17	18	19	20	21	22	23	24	25	26	27	
	G9619/16	G9619/16	G9619/20	G9620/6	G9620/6	G9620/9	G9621/1	G9621/1	G9621/1	G9621/4	G9621/4	G9624/15	G9624/15	
SiO_2	48.49	50.97	45.51	46.81	46.66	46.46	45.00	45.61	46.59	46.55	46.59	46.86	52.91	
Al_2O_3	32.48	30.26	33.83	34.18	34.26	33.74	33.82	33.75	33.54	33.48	33.56	33.12	29.64	
FeO	0.33	0.60	0.79	0.36	0.28	0.43	0.83	0.76	0.79	0.65	0.71	0.22	0.86	
MgO	0.00	0.00	0.00	0.00	0.00	0.00	0.00	0.00	0.00	0.00	0.00	0.00	0.00	
CaO	16.38	14.54	18.22	17.64	17.21	17.89	18.02	18.17	17.11	17.88	17.54	17.25	12.71	
Na_2O	1.98	3.02	0.86	1.12	1.25	1.44	1.09	0.72	0.94	1.05	1.09	1.38	3.51	
K_2O	0.00	0.08	0.02	0.00	0.00	0.00	0.09	0.00	0.09	0.00	0.08	0.00	0.04	
Total	99.66	99.47	99.23	98.99	99.66	99.96	98.85	99.01	99.06	99.61	99.57	98.83	100.10	
An	81	72	91	89	85	88	90	91	86	89	87	86	67	

Notes: 1–6, 12, 17–23 – phenocrysts; 14, 15 – phenocryst core and rim, respectively; 7 – microphenocryst; 8–11, 13, 16 – microlites. Measured on a Cam Scan microprobe with a Link 860 analyzer and a Link 1000 processor. Accelerating voltage 20 kV, current 10^{-9} A. 150-eV-resolution Si (Li) semiconductor detector.

It is likely that, formerly, part of the Spiess caldera emerged above sea level, as suggested by the pneumatolytically metasomatized rocks with oxidized groundmass. Owing to vigorous postvolcanic activity, scoria and basalts in the vicinity of the caldera experienced oxidation and hydrothermal alteration.

A petrographic description of volcanics from the *SWIR segment located southeast of the Bouvet TJ,* including the rift valley (St. S1815–17, 22–27, 30, 31, 36, 37), ridge flanks (St. S1828, 29, 32, 33, 35, 40–44), and slopes of the Bouvet Rise (St. S1813, 14, 19–21), was given in a previous study [*Peyve et al.,* 1995]. Importantly, the rocks dredged from the rise slope are similar to those recovered from the Spiess caldera slopes. Their significant distinction is the large amount of shingles, from which the volcanic samples were obtained, and the relatively large proportion of metabasalts (S1814/51–56, S1821/31) containing chlorite and sulfides, which point to a tectono-volcanic nature for the rise forming the Bouvet I. Basalts dredged from the rift valley are dominated by moderately to weakly vesicular varieties. At the intersection of the rift valley and the rise forming the Bouvet I., the role of rounded material and strongly vesicular volcanites increases. The flank basalts generally match those from the rift valley in diversity, but they have a greater proportion of altered varieties.

The Bouvet Fracture Zone was sampled thoroughly on Cruise 18 by a long dredging traverse (St. S1806–S1812). It is noteworthy that the dredged basalts are dominantly non- or weakly vesicular, with altered varieties containing chlorite, smectite, and carbonates. Stations S1807 and S1810 yielded a minor amount of strongly vesicular volcanics, including some that resembled volcanic bombs.

On the *Mid-Atlantic Ridge,* detailed sampling covered the rift valley (St. S1848–S1853, S1861–S1864, G9624–G9626) (Figure 1, Table 1). Fresh non-vesicular or weakly vesicular, aphyric and strongly phyric basalts were recovered. The phenocryst assemblage is dominated by plagioclase. In basalts from St. G9626, plagioclase accounts for as much as 30%. Olivine is less abundant, and clinopyroxene is encountered even more seldom. The measured plagioclase and olivine phenocryst compositions are An_{86} and Fo_{78-80}. The plagioclase and clinopyroxene microlite compositions measured from Sample G9624/15 are, respectively, An_{67} and Fs_{21} (Tables 2, 3, 4). Of secondary minerals, only glauconite is de-

Table 3. Electron microprobe analyses of olivines

	1	2	3	4	5	6	7	8	9	10	11	12
	G9608/27	G9608/48	G9608/48	G9608/48	G9608/48	G9608/55	G9608/55	G9609/16	G9609/16	G9609/16	G9609/16	G9616/4
SiO_2	38.25	37.84	37.05	37.37	37.53	37.28	37.54	40.02	39.55	39.50	40.02	40.00
FeO	19.05	24.98	28.57	30.08	29.49	24.32	32.03	17.07	16.34	16.38	15.92	13.22
MnO	0.39	0.32	0.37	0.38	0.41	0.36	0.56	0.26	0.11	0.17	0.20	0.19
MgO	41.38	37.24	34.16	33.84	33.53	36.31	30.23	43.60	42.75	45.00	44.75	46.20
CaO	0.26	0.00	0.37	0.00	0.33	0.15	0.30	0.32	0.24	0.27	0.20	0.24
Total	100.51	100.39	100.64	101.67	101.29	98.42	100.66	101.27	98.99	101.32	101.09	99.85
Fo	79.47	72.65	68.06	66.72	66.95	72.68	62.71	81.99	82.34	83.04	83.36	86.16
	13	14	15	16	17	18	19	20	21	22	23	
	G9619/16	G9619/16	G9619/16	G9619/20	G9620/6	G9620/9	G9621/4	G9621/4	G9624/2	G9624/2	G9624/15	
SiO_2	39.99	38.97	39.10	37.35	40.00	39.51	38.43	38.37	39.15	38.85	38.32	
FeO	12.47	17.14	15.99	29.13	15.19	16.08	21.01	21.34	18.92	19.14	20.43	
MnO	0.10	0.20	0.25	0.57	0.23	0.19	0.34	0.46	0.29	0.45	0.24	
MgO	46.65	42.55	43.82	32.07	45.79	43.97	39.59	38.99	41.88	41.21	40.58	
CaO	0.28	0.46	0.28	0.17	0.31	0.35	0.28	0.34	0.34	0.21	0.33	
Total	99.49	99.32	99.44	99.29	101.52	100.10	99.65	99.50	100.58	99.86	99.90	
Fo	86.96	81.56	83.01	66.24	84.31	82.97	77.05	76.51	79.78	79.33	77.97	

Notes: 1–3, 6, 9–13, 18–23 – phenocrysts; 4, 5, 7, 8, 14–17 – microphenocrysts.

veloped in minor amounts in the dark-colored halo zones in the pillows (Table 5). The flanks of this ridge were sampled at three stations (S1857, S1866, S1867). Basalts recovered were described in previous works [*Peyve et al.,* 1995] and, unlike the rift basalts, these are noted for strong secondary alterations.

On the southwest flank of the MAR, the *Shona Rise* is situated, which was sampled at two stations: G9608 near the summit of a conical edifice and G9609 from the ridge slope, on which this edifice is located (Figure 1, Table 1). The volcanic material obtained, covering a broad lithological range from basalt to rhyolite, resembles largely in aspect the Spiess Ridge volcanics in that it is also dominated by vesicular varieties. The least vesicular basalts fall into two groups in terms of their alteration products. One group comprises basalts with alteration products such as smectite, zeolites, chlorite, and actinolite (G9608/3, 4, 45, 48, 52, G9609/2), i.e., relatively deep-seated secondary minerals, with Sample G9609/2 bearing evidence of having been broken freshly off the slope. These are porphyritic varieties with noticeable contents (4–8%) of Ol+Pl+Cpx (G9608/3), Ol alone (G9608/48, G9609/16), or Pl alone (G9608/45, 52, G9609/2). From Samples G9608/48 and G9609/16, olivine compositions (Fo_{69-73} and Fo_{82-83}, respectively), and from G9609/16, a plagioclase microphenocryst composition (An_{60}) (Tables 2, 3) were measured. The other group includes weakly vesicular fresh basalts, occasionally with minor amounts of a Fe-hydroxide and glauconite-like minerals (G9608/5, 51, 55, G9609/3, 5, 10, 16) that form, as a rule, in near-bottom environments. This group includes aphyric (G9608/51, G9609/3, 5) and porphyritic varieties with Opx, Cpx, Pl (G9608/5, G9609/10) and with Ol and Pl (G9608/55). Phenocryst compositions have been measured; they are An_{87-92} for plagioclase, Fs_{16} for clinopyroxene, Fs_{26-30} for orthopyroxene, and Fo_{73} for olivine. An olivine microphenocryst from Sample G9608/55 yielded Fo_{63} (Tables 2, 3, 4).

The strongly vesicular varieties are dominated by volcanics that are more silicic than basalt. The most vesicular rocks represent volcanic scoria, some samples displaying odd forms resembling volcanic bombs. Many volcanics in this group are reddish to intense red in color due to an oxidized matrix, hyalopilitic in texture, or to Fe-hydroxide precipitation on vesicle walls. These include aphyric (G9608/8, 13, 15, 25, 28, 37, 42, 43, G9609/18) varieties with sporadic Cpx, Pl, and Pl+Px+Ol phenocryst assemblages (G9608/27, 29, G9609/11) and Pl-phyric varieties (G9608/31). In the phenocryst assemblage from the dacitic andesite G9608/58, plagioclase is accompanied by hornblende. In strongly oxidized rocks, the olivine phenocrysts are opacitized. Tables 2, 3, and 4 list the compositions of some plagioclase (An_{86-96}), clinopyroxene (Fs_{19}), orthopyroxene (Fs_{39}), and olivine (Fo_{79}) phenocrysts.

The textural and structural characteristics of the dredged volcanics thus suggest a tectono-volcanic nature for the Shona Rise. Supposedly, the central-type volcanic edifice

Table 4. Electron microprobe analyses of pyroxenes

	1	2	3	4	5	6	7	8
	G9608/5	G9608/5	G9608/27	G9608/42	G9609/10	G9609/10	G9610/30	G9610/30
SiO_2	50.90	54.15	52.84	51.57	52.24	53.15	44.21	44.54
TiO_2	0.31	0.16	0.13	0.36	0.25	0.16	5.32	5.05
Cr_2O_3	0.13	0.01	0.12	0.16	0.17	0.00	0.13	0.20
Al_2O_3	2.27	0.43	0.29	2.04	1.38	0.79	6.71	6.56
FeO	10.59	16.89	24.34	11.94	19.13	18.42	11.48	10.23
MnO	0.24	0.42	0.44	0.16	0.57	0.52	0.16	0.06
MgO	15.18	25.50	19.86	15.77	23.65	24.15	9.02	10.79
NiO	0.00	0.00	0.00	0.00	0.00	0.00	0.00	0.00
CaO	20.72	1.62	2.05	17.83	1.99	1.70	22.02	22.11
Na_2O	0.00	0.00	0.00	0.00	0.00	0.00	0.00	0.00
K_2O	0.00	0.00	0.00	0.00	0.00	0.00	0.00	0.00
Total	98.07	99.18	100.07	99.83	99.38	98.89	99.05	99.54
Fs	16	26	39	19	30	29	20	18
En	42	71	57	45	66	68	29	33
Wo	42	3	4	36	4	3	41	49
	9	10	11	12	13	14	15	16
	G9612/30	G9617/1	G9619/20	G9619/20	G9619/20	G9620/6	G9621/1	G9624/15
SiO_2	52.27	45.63	51.47	51.77	51.46	51.48	52.32	45.63
TiO_2	1.12	4.27	0.48	0.40	0.41	1.31	0.46	2.75
Cr_2O_3	0.00	0.11	0.05	0.00	0.08	0.63	0.15	0.14
Al_2O_3	2.45	7.17	3.36	2.84	3.54	5.66	2.10	6.65
FeO	12.42	9.68	8.26	9.03	8.28	6.26	9.11	12.11
MnO	0.27	0.11	0.32	0.14	0.14	0.12	0.35	0.13
MgO	13.69	10.52	13.37	14.52	13.82	16.51	15.30	10.61
NiO	0.00	0.00	0.00	0.00	0.00	0.00	0.00	0.00
CaO	19.83	22.21	22.28	20.89	22.47	20.81	19.96	21.69
Na_2O	0.00	0.00	0.00	0.00	0.00	0.00	0.00	0.00
K_2O	0.00	0.00	0.00	0.00	0.00	0.00	0.00	0.00
Total	102.05	99.70	99.59	99.59	100.20	102.78	99.75	99.71
Fs	20	17	14	15	14	10	15	21
En	39	33	39	42	40	47	44	32
Wo	41	50	47	43	46	43	41	48

Notes: 1, 4, 9, 11–13, 15 – clinopyroxene phenocrysts; 14 – clinopyroxene microphenocryst; 7, 8, 10, 16 – clinopyroxene microlites; 2, 3, 5, 6 – orthopyroxene phenocrysts.

in the making had at its base a sequence composed of non-vesicular diagenetically altered basalts. These basalts are now exposed at the ocean floor due to subsequent tectonic movements. That these movements had a great magnitude is evidenced by gabbros dredged alongside basalts. As the volcanic edifice was growing in height, increasingly more vesicular volcanics formed. By analogy with the Spiess Ridge, it would be sensible to assume that the volcanic summit emerged above sea level. This is further supported by the rounding of some of the samples and the flattened top of the rise, possibly owing to abrasion.

On the *America-Antarctic Ridge,* only the inner corner high was sampled, yielding a minor amount of volcanic material. Dredged were the lower, middle, and upper portions of the slope (St. G9602, G9604, and G9605, respectively; Figure 1, Table 1). The volcanics include (i) weakly vesicular, chiefly aphyric, altered basalts with chlorite or smectite as secondary phases and represented by small rounded debris (G9602/1–4, 11–15, G9604/49, 51, 53-56), (ii) strongly vesicular aphyric basaltic andesites, occasionally forming volcanic bombs (G9602/5–7, G964/50, 52, 76, 77), and (iii) dacites with a minor amount of small plagioclase and hornblende phenocrysts (G9605/1). Dacites have been encountered as poorly rounded debris enclosed in a breccia with a clay/sand matrix.

The dredge from the upper part of the slope also recovered gabbros and ultramafites, emplaced at this level due to intense tectonism. Presumably, the top of the rise once occurred above sea level, as evidenced by its abraded character and the fact that most of the rocks just mentioned were recovered as shingles. The sampled strongly vesicular basaltic andesites and dacites likely point to central-type volcanism as a causative mechanism for the conical edifice on the west end of the corner high.

Table 5. Electron microprobe analyses of secondary minerals

	1	2	3	4	5	6	7	8	9	10
Mineral	G9610/2 Glauconite	G9610/2 Glauconite	G9614/10 Glauconite	G9614/10 Glauconite	G9614/25 Glauconite	G9619/16 Glauconite	G9620/6 Glauconite	G9620/9 Glauconite	G9620/9 Glauconite	G9624/2 Glauconite
SiO_2	46.59	46.33	45.78	46.71	41.48	48.79	50.24	49.54	50.30	47.96
TiO_2	0.07	0.00	0.15	0.39	0.02	0.00	0.09	0.04	0.00	0.09
Cr_2O_3	0.00	0.11	0.00	0.00	0.03	0.00	0.00	0.13	0.16	0.65
Al_2O_3	1.75	1.99	3.59	3.75	9.07	1.90	3.66	5.29	0.54	0.72
FeO	33.86	33.03	23.75	25.97	19.03	28.93	26.47	27.26	27.84	30.12
MnO	0.00	0.00	0.00	0.07	0.22	0.00	0.01	0.00	0.01	0.08
MgO	2.78	2.55	2.92	2.86	12.01	3.88	4.69	4.06	4.21	2.93
NiO	0.00	0.00	0.00	0.00	0.00	0.00	0.00	0.00	0.00	0.00
CaO	0.80	0.58	0.62	0.87	0.43	0.59	0.53	0.39	0.40	0.33
Na_2O	0.54	0.54	0.00	0.60	0.00	0.61	0.23	0.00	0.00	0.00
K_2O	4.50	5.26	3.83	3.72	5.24	5.08	5.47	6.30	6.88	5.64
Total	90.89	90.40	80.63	84.94	87.54	89.78	91.38	93.01	90.34	88.51
	11	12	13	14	15	16	17	18	19	20
Mineral	G9610/30 Smectite	G9614/35 Nontronite	G9614/35 Nontronite	G9612/34 Chlorite	G9617/12 Chlorite	G9617/12 Chlorite	G9617/14 Chlorite	G9612/6 ?	G9616/4 ?	G9617/14 Ankerite
SiO_2	51.49	50.65	49.10	35.61	31.09	30.73	32.98	46.13	59.01	0.39
TiO_2	0.14	0.67	0.98	0.13	0.06	0.07	0.10	2.84	0.06	0.05
Cr_2O_3	0.11	0.00	0.00	0.80	0.05	0.21	0.18	0.14	0.07	0.00
Al_2O_3	6.70	4.06	4.46	17.49	18.13	18.15	12.94	3.98	19.85	0.00
FeO	16.28	27.71	27.95	18.84	20.22	21.00	16.00	16.57	0.91	7.41
MnO	0.11	0.00	0.00	0.12	0.32	0.22	0.26	0.41	0.11	0.41
MgO	17.37	2.54	2.25	16.60	20.52	19.45	17.62	11.50	0.00	10.75
NiO	0.00	0.00	0.00	0.00	0.00	0.00	0.00	0.00	0.00	0.00
CaO	1.13	0.52	0.63	0.56	0.22	0.18	0.53	14.85	0.10	28.40
Na_2O	0.64	0.65	1.33	0.18	0.05	0.00	0.00	1.31	3.56	0.00
K_2O	2.63	2.81	2.78	0.19	0.00	0.03	0.00	0.06	7.04	0.03
Total	96.59	89.62	89.49	90.54	90.67	90.05	80.62	97.78	89.88	47.43

Notes: 1–10 – glauconites forming thin green-colored fringes on vesicle walls near contraction joints in pillows; 11 – high-Fe saponite filling up vesicles completely; 12, 13 – nontronites filling in vesicles and replacing glassy groundmass in basalts; 14–17 – chlorites filling in vesicles and partly replacing basaltic groundmass, including plagioclase and clinopyroxene microlites; 18, 19 – finely dispersed aggregates localized on vesicle walls in oxidized basalts; 20 – ankerite from a large vesicle.

The area in which the *America-Antarctic and Southwest Indian Ridge fossil structures converge* is structurally complex because of overprinted within-plate tectonic movements [*Skolotnev,* 2000]. Of the four dredges from this area, two (G9620 and G9621) characterize the walls of the passive portion of the Bouvet FZ, one (G9619) sampled a minor rise that belongs to the America-Antarctic Ridge, and yet another one (G9610), the slope of a rise representing a relict structure of the MAR (Figure 1, Table 1).

Station G9610 yielded weakly vesicular (2–4%, rarely up to 10% vesicles) aphyric (Smp. G9610/1–15, 17, 23, 29–36) and Ol-Pl phyric (G9610/16, 18–22, 24–28) basalts. Some of the rocks are very fresh, resembling those dredged from the MAR rift valley (G9610/1–12). The others are more or less altered. Thus, G9610/30 exhibits smectite compositionally close to saponite (Table 5). From the same sample, clinopyroxene microlites with a clear pink coloring were measured, yielding Ti-augite with high TiO_2 abundances (5.05–5.32%) (Table 4).

At St. G9619, basalts are distinguished by a broad structural and textural diversity. The following varieties are recognized: non-vesicular Pl-phyric (G9619/1–4, 23), vesicular (15–20%) aphyric (G9619/10–14), and Ol-Pl phyric (G9619/5–9, 15, 16). Alongside basalts, dredged were more silicic volcanics with Ol, Cpx, Pl and, at times, Hb phenocrysts, distinctive for their strong vesiculation (up to 80%;

Table 6. Electron microprobe analyses of titanomagnetites

	1	2	3	4	5	6
	G9608/27	G9608/55	G9609/10	G9610/30	G9619/20	G9621/4
SiO_2	0.73	0.48	0.72	0.59	0.57	0.61
TiO_2	10.56	15.59	7.58	29.91	9.74	13.75
Cr_2O_3	0.22	0.35	0.72	0.32	0.14	0.03
Al_2O_3	3.21	1.52	4.47	1.69	4.29	2.27
FeOsum	76.78	76.62	78.90	67.09	78.90	77.33
MnO	0.22	0.29	0.22	0.65	0.27	0.49
MgO	2.91	0.57	0.66	1.67	2.62	1.41
Total	94.63	95.42	93.27	101.92	95.42	95.89

Samples G9619/18–21). The measured phenocryst compositions from a basalt (G9619/16) and a more silicic volcanic rock (G9619/20) differ noticeably. From Smp. G9619/16, microprobe measurements on a plagioclase phenocryst gave An_{89} (core) and An_{81} (rim), An_{72} on a microlite, Fo_{85-87} on an olivine phenocryst, and Fo_{82} on an olivine microphenocryst. From Smp. G9619/20, Pl is An_{91}, Ol is Fo_{66}, and Cpx is Fs_{14-15} (Tables 2, 3, 4). Of secondary minerals, glauconite (Table 5) and smectite have been detected.

Volcanic materials recovered from Sts. G9620 and G9621 are similar. The basalts also include non-vesicular aphyric (G9620/10–12, 18, 19, G9621/6, 7, 10–12) and Ol-Pl phyric (G9620/1–9, 13–17, G9621/4, 5, 9) and vesicular (10–15%) aphyric (G9620/21, 22, G9621/1, 2) and Pl-phyric (G9621/3) varieties. The aphyric varieties display sporadic Pl, Ol, and Cpx phenocrysts. St. G9620 also yielded strongly vesicular (60–80%) rocks, represented by oxidized red-colored scoria (G9620/25–27) and volcanic bombs (G9620/23, 24, 28). The latter are felsic (to dacite inclusive) and contain minor Pl, Ol, and Cpx phenocrysts. Phenocryst compositions were measured from four samples, and they fall into two groups irrespective of their structural or textural characteristics. Smps. G9620/6, 9 yielded An_{85-89}, Fo_{83-84}, Fs_{10}, and Smps. G9621/1, 4 yielded An_{85-91}, Fo_{76}, Fs_{15} (Tables 2, 3, 4). Most volcanics are slightly altered, showing only minor amounts of glauconite (Table 5). A number of samples are tectonized and contain chlorite (G9620/7, 20).

Basalts from the *zone in which the AAR and MAR converge* (St. S1854 to 56) are overall close to those from the MAR flanks.

The area in which the MAR and SWIR fossil structures converge has been sampled at a single station, G9617 (Figure 1, Table 1), confined to a tectonic scarp making up the wall of one of a number of graben-like depressions. The dredged basalts, mostly aphyric and virtually non-vesicular, differ from each other in freshness. Some bear only superficial alteration products (palagonite) (G9617/1 to 11), while others contain noticeable amounts of chlorite, some carbonates (Table 5), quartz, pyrite and occasional chalcopyrite and bornite (G9617/12 to 33) and are thus likely to come from the lower horizons in the basaltic pile. The chlorite-bearing basalts are tectonized and cut by numerous cleavage joints.

Three stations (G9618, 22, 23) sampled *three separate ridges extending between the Spiess Rise and Bouvet I.* (Figure 1, Table 1). The rocks obtained are uniform and similar to those exposed on the rises just mentioned. These are mostly vesicular to strongly vesicular, sparsely Ol-Pl phyric basalts and more silicic volcanics. Some of them are red-colored due to strong oxidation, while others are noticeably palagonitized (G9623/1, 2). A minor proportion of the basalts are vesicular and more strongly altered, to the degree where smectite appears (G9618/7, G9622/6).

Listed above were phenocryst and microlite compositions from some of the volcanics. The number of measurements is not sufficient for valid conclusions concerning the character of variations in the modal compositions, although certain trends are readily identifiable.

The highest-Fe olivine phenocrysts are encountered among the Shona Rise volcanics. Large phenocrysts are Fo_{72-80}, and fine are Fo_{62-67}. Olivines like this are found in similar volcanites from the other structures in the area where the MAR, SWIR, and AAR fossil structures come together. Remarkably, the highest-Fe olivine phenocrysts are associated with the most calcic plagioclase phenocrysts, An_{86-96}. The most magnesian olivine phenocrysts (Fo_{86-87}) occur in depleted basalts, in which plagioclase phenocrysts are generally more sodic (An_{85-89}) than on the Shona Rise. Orthopyroxene phenocrysts occur only in the Shona Rise volcanics and in their counterparts. All the clinopyroxene microlites studied differ from the phenocrysts in having greater Fe-numbers and are high in TiO_2, which increases with the degree of enrichment of the basalts. The opaque phenocrysts measured correspond to Ti-magnetite (Table 6). Noticeably greater TiO_2 abundances (29.91%) mark the grains from Smp. G9610/30, which also represents basalts that contrast in composition to the other rocks. Several spinel grains were analyzed from these volcanics. The covariation of their Cr-number (40–51) and Mg-number (40–70) places these spinels in the mantle peridotite array, although their high TiO_2 abundances point to interaction with a basaltic melt (Table 7).

Volcanic Rock Chemistry

Volcanic rock chemistries from the Bouvet TJ were studied by a number of marine expeditions [*Dick et al.*, 1984; *Dickey et al.*, 1977; *Le Roex et al.*, 1983, 1985, 1987]. Lava

Table 7. Electron microprobe analyses of spinels

	1	2	3	4
	G9609/16	G9617/1	G9620/9	G9624/15
SiO_2	0.52	0.24	0.68	0.23
TiO_2	3.07	0.88	1.33	0.42
Cr_2O_3	28.17	32.42	36.61	35.99
Al_2O_3	26.43	32.81	23.16	28.67
FeOsum	31.58	17.71	26.74	17.61
MnO	0.12	0.07	0.06	0.00
MgO	9.63	15.78	12.32	16.01
Total	99.52	99.91	100.90	98.93
Mg#	41	67	53	70
Cr#	42	40	52	46

compositions were found to cover a wide range from picrite to ferrobasalt. The upwelling Bouvet mantle plume has been shown to generate in its immediate vicinity basaltic provinces enriched in LREE and with $^{87}Sr/^{86}Sr$ and $^{143}Nd/^{144}Nd$ ratios either greater or lower than in N-MORB. These conclusions are based chiefly on the study of basalts from the axial parts of the mid-oceanic ridges. We will address basaltic compositions from a variety of structural settings that cover a much larger area, thereby enabling the analysis of volcanism in this region over a considerably longer time span.

Basalts of the southern part of the MAR (Table 8) within its axial (rift) zone are comparatively uniform in composition. These are mostly fresh, poorly to moderately fractionated N-MORB-like tholeiitic basalts ($(La/Sm)_n$ = 0.7–1.0, $(Nb/Zr)_n$ = 0.3–0.7)) with FeO^*/MgO chiefly in the range 1.2–1.4 (hereafter, the $(La/Sm)_n$ ratios are from [*Pushcharovsky et al.,* 1998; *Simonov et al.,* 1996; *Sushchevskaya et al.,* 1999]). Their TiO_2, K_2O, and P_2O_5 abundances increase systematically from 1.1%, 0.2%, and 0.08% in the least evolved rocks (Smp. G9625/1 with FeO^*/MgO = 0.8) to 2.2%, 0.4%, and 0.6%, respectively, in the most evolved basalts with FeO^*/MgO = 1.7–1.8 (Figures 2–4). The rocks are fresh, with loss on ignition (LOI) of less than 1%. They contain 48–50% SiO_2, 130–150 ppm Cr, 90–150 ppm Sr, and 1–10 ppm Rb. Basalts from St. G9624 are distinctive in having considerably greater K_2O (up to 0.57%) and P_2O_5 (up to 0.24%), which places them with T-MORB.

In the variation diagrams, the Mid-Atlantic Ridge basalts, except for the notably altered varieties, plot in compact clusters or along trends, their greatest distinction from the other volcanics from this area being the higher FeO^* and lower Al_2O_3 values for equivalent fractionation indices, FeO^*/MgO, and the lower rate of K_2O enrichment (Figures 2, 4).

The Spiess Ridge is composed of fresh, dominantly vesicular basalts and basaltic andesites (Table 8). Unlike the MAR basalts, they span a much larger range from poorly fractionated rocks with FeO^*/MgO = 1.1 to strongly evolved varieties with FeO^*/MgO = 4, dominant values ranging from 1.8 to 2.5. The TiO_2 vs. FeO^*/MgO plot (Figure 2) shows clearly a fractionation trend with TiO_2 increasing sharply from 2.16% (G9612/19) to 3.43% (G9614/20). In further melt fractionation, massive oxide crystallization causes a drop in TiO_2 to 2.5% at FeO^*/MgO of ca. 4 (G9612/6). With progressive fractionation, as appears from the oxides vs. FeO^*/MgO plot (Figure 2), SiO_2 increases from 45 to 55%; K_2O, from 0.4 to 1.6%; P_2O_5, from 0.1 to 0.65%; and Na_2O, from 2 to 6%. The Al_2O_3 abundances decrease systematically from 17 to 14% and CaO, from 12 to 6%. Data points for basalts from the Spiess Ridge are readily approximated by a single differentiation trend, which suggests a constancy of magmagenesis parameters over the entire length of the ridge and throughout its lifetime. The homogeneity of the mantle source is supported by the narrow variation ranges of lithophile element ratios such as $(La/Sm)_n$ = 1.6–2.1 and $(Nb/Zr)_n$ = 0.8–1.2. Note that this same trend accommodates the volcanics from all the sampled structural features of the ridge irrespective of their structural or petrographic distinctions. This applies equally to the weakly vesicular varieties, vesicular lavas, pillows, and extremely vesicular scoria. The least evolved sample from the Spiess Ridge, G9612/19, in terms of its SiO_2, K_2O and P_2O_5 concentrations is close to the enriched basalts from the MAR rift valley (St. G9624), although it differs from them in having lower Cr, Cu, Ni, V, Zn, Co, and Sc. These elements, particularly Cr, exhibit moderate to depleted concentrations in all the Spiess Ridge volcanics.

Among all the Spiess Ridge basalts, Smp. G9614/22 is outstanding by many parameters; thus, its $(Nb/Zr)_n$ ratio is as low as 0.38, and its TiO_2 and Na_2O abundances are very low. These traits make it similar to the Shona Rise basalts, which are considered below. Another exception is Smp. G9614/10, noted for its considerably depressed Na_2O and very high Cr (ca. 250 ppm), rendering it similar to the enriched basalts encountered on the MAR.

Our dredges from the *slopes of the Bouvet I.* recovered basalts and basaltic andesites. Chemically similar rocks are widespread on Bouvet I. proper as well. In [*Le Roex and Erlank,* 1982], these rocks based on their subalkaline trend are classified as hawaiites and mugearites, names we will hereafter apply. In terms of many components, including primarily such genetically important ones as TiO_2, K_2O, and P_2O_5, most hawaiites and mugearites from Bouvet I. and its submarine slopes fit with a coherent extensive differentiation trend, corresponding to that for the Spiess Ridge volcanics. Unlike the latter, however, it is much more evolved, as evidenced by very silicic volcanics inclusive of rhyolite encountered on the island [*Le Roex and Erlank,* 1982]. The hawaiites and mugearites show FeO^*/MgO from 1 to 5, SiO_2 ranging from 48% to 55%, TiO_2 increasing from 2.28% to 4.4% and then dropping to 1.52% in the most evolved rocks, K_2O ranging from 0.8% to 2.3%, and P_2O_5, from 0.4% to 1.0% [*Le Roex and Erlank,* 1982; *Simonov et al.,* 2000]. Further distinctions between the Spiess Ridge and Bouvet I. volcanites are as follows. In the SiO_2, FeO^*, Na_2O, and Al_2O_3 vs. FeO^*/MgO covariation plots, Bouvet I. data points make up independent trends at lower SiO_2, FeO^*, and Na_2O and higher Al_2O_3 values relative to the Spiess Ridge volcanic suite, but parallel to its trends (Figures 2, 3, and 4). The basalts display strongly variable alteration degrees (0.1–2.4% LOI). On the other hand, the K_2O vs. LOI plot (Figure 5), e.g., reveals

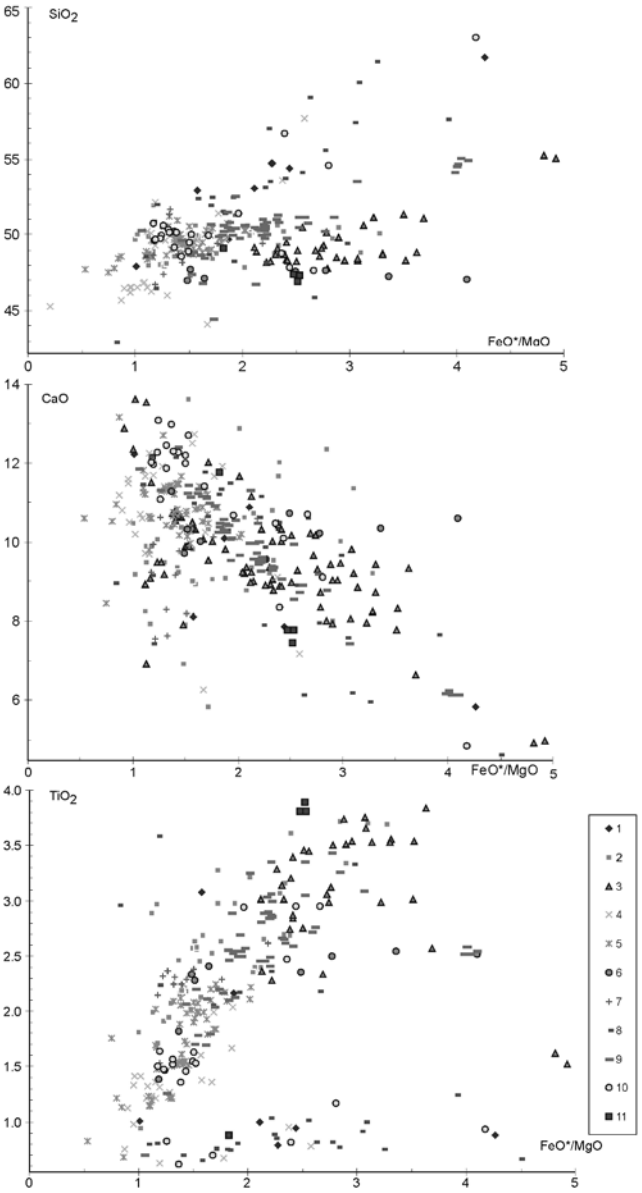

Figure 2. SiO_2, CaO, and TiO_2 vs. FeO^*/MgO plots for basalts. 1 – America-Antarctic Ridge, 2 – Southwest Indian Ridge, 3 – Bouvet I., 4 – Bouvet FZ., 5 – Mid-Atlantic Ridge, 6 – rise between the two troughs into which the south tip of MAR bifurcates (St. G9610), 7 – East Dislocation Zone, 8 – Shona Smt., 9 – Spiess Ridge, 10 – zone of convergence of the America-Antarctic, Southwest Indian, and Mid-Atlantic ridges, 11 – linear rise between Bouvet I. and Spiess Ridge (St. G9622). Data used are from this study and from [*Dickey,* 1977; *Didenko et al.,* 1999; *Le Roex and Erlank,* 1982; *Le Roex et al.,* 1983, 1987; *Pushcharovsky et al.,* 1998; *Simonov et al.,* 1996, 2000].

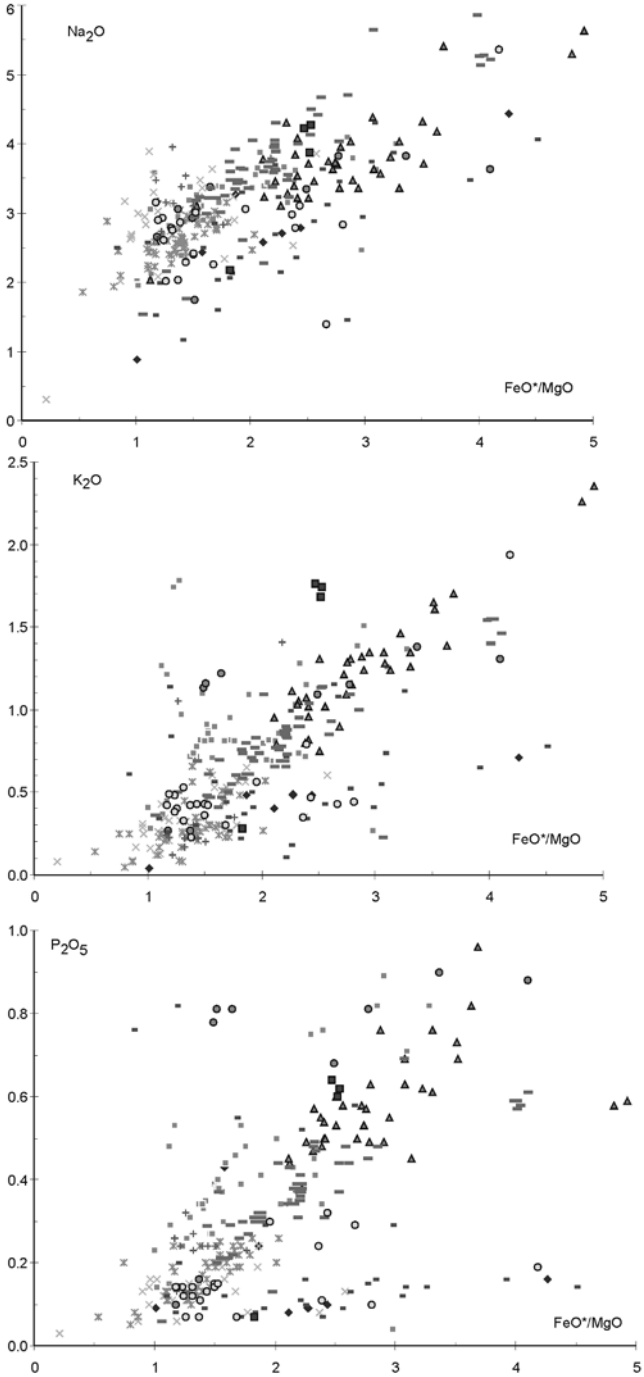

Figure 3. Na_2O, K_2O, and P_2O_5 vs. FeO^*/MgO plots. For symbols, see Figure 2.

a lack of significant correlation between the two parameters, which enables us to use lithophile element abundances for a comparative characterization of magmatic processes. A number of lithophile trace elements show variation patterns similar to those from the Spiess Ridge basaltic rocks. However, the most evolved volcanics from Bouvet I., no counterparts of which have been encountered on the Spiess Ridge, exhibit greater incompatible element ratios ($(La/Sm)_n = 2–3$ [*Le Roex and Erlank,* 1982; *Simonov et al.,* 2000], $(Nb/Zr)_n = 1.4–1.7$, $Zr/Y \sim 7.3$). Of the other trace elements, Cr and Ni are typically very low, rendering these rocks similar to the Spies Ridge volcanics but sharply contrasting to the other basalts from this region.

Table 8. Chemical compositions of basalts

Sample no.	SiO_2	TiO_2	Al_2O_3	FeO	MnO	MgO	CaO	Na_2O	K_2O	P_2O_5	Cr_2O_3	LOI	Total	Cr	Cu	Ni	Sr	V	Zn	Zr	Co	Y	Sc	Nb	FeO^*/MgO
G9602/03	49,69	2,16	13,82	12,28	0,206	6,57	10,10	3,27	0,48	0.24	0.02	1.18	100.01							150				5.8	1.87
G9604/50	54.69	0.79	15.94	11.01	0.208	4.84	9.55	2.71	0.48	0.09	0.01	0.00	100.32							40				1.1	2.27
G9604/50	54.74	0.79	15.96	11.02	0.208	4.84	9.56	2.71	0.49	0.09	0.01	0.00	100.42												2.28
G9604/52	54.38	0.94	15.29	11.17	0.227	4.58	7.85	2.79	0.48	0.10	0.01	1.91	99.73	480	152		191	357	178	107	17	13	45		2.44
G9604/54	52.95	3.08	11.62	10.06	0.139	6.38	8.12	2.44	3.01	0.43	0.03	1.93	100.19	615	94	63	1060	248	121	318	19	17	26		1.58
G9604/56	47.89	1.01	16.70	9.46	0.182	9.39	12.22	0.88	0.04	0.09	0.04	2.60	100.50												1.01
G9604/76	53.04	1.00	17.04	10.02	0.185	4.75	10.88	2.57	0.40	0.08	0.01	0.25	100.23												2.11
G9605/01	61.69	0.88	15.48	8.70	0.226	2.04	5.84	4.43	0.71	0.16	0.01	0.00	100.16	195	27		170	80	140	108	9	21	31		4.26
G9608/03	42.93	2.96	10.93	12.01	0.173	14.71	8.95	2.49	0.61	0.76	0.07	3.45	100.04							280				67	0.82
G9608/04	49.44	3.33	12.97	14.29	0.24	4.82	9.67	2.95	0.41	0.29	0.01	0.80	99.24												2.96
G9608/05	54.11	1.02	15.73	11.09	0.24	4.36	8.91	2.88	0.43	0.09	0.01	0.00	98.87							46				1	2.54
G9608/08	67.05	0.77	17.62	5.17	0.049	1.83	0.51	1.46	3.74	0.16	0.01	2.13	100.50							180				1	2.83
G9608/13	57.64	1.24	13.88	12.38	0.227	3.17	7.66	3.47	0.65	0.16	0.01	0.00	100.49												3.91
G9608/15	48.20	2.36	14.84	10.57	0.377	4.80	11.16	3.69	0.72	0.52	0.01	3.01	100.26	535	74	96	385	328	191	245	64	34	40		2.20
G9608/24	45.86	2.18	13.52	12.46	0.840	4.70	10.60	3.12	1.08	0.58	0.01	4.04	98.99												2.65
G9608/25	50.88	0.81	16.30	9.51	0.198	8.23	12.16	1.52	0.26	0.08	0.02	0.22	100.19							27				1	1.16
G9608/27	52.45	0.81	18.55	8.99	0.20	4.75	10.29	2.36	0.50	0.09	0.01	0.15	99.15												1.89
G9608/28	60.06	1.00	16.11	7.87	0.21	2.56	6.18	4.31	0.74	0.14	0.01	0.55	99.74												3.07
G9608/29	57.01	0.89	17.46	8.06	0.180	3.61	7.91	3.23	0.99	0.16	0.01	0.80	100.31							86				1.8	2.23
G9608/31	55.59	0.82	15.74	9.96	0.248	3.61	7.95	3.45	0.52	0.15	0.01	0.92	98.97												2.76
G9608/37	57.42	0.92	15.34	10.42	0.237	3.43	7.57	3.74	0.55	0.12	0.01	0.49	100.25							49				1	3.04
G9608/43	61.43	0.75	14.40	8.23	0.197	2.54	5.95	3.88	1.11	0.14	0.01	0.45	99.08							120				3.1	3.24
G9608/45	53.15	1.03	14.48	11.63	0.183	5.29	10.63	2.69	0.11	0.11	0.01	0.67	99.98							61				2.1	2.20
G9608/46	52.01	2.24	10.04	11.60	0.159	9.77	7.43	1.99	0.84	0.20	0.06	3.55	99.89							130				5.5	1.19
G9608/48	46.47	3.58	12.56	12.70	0.166	10.78	9.15	2.64	1.14	0.82	0.03	0.00	100.04												1.18
G9608/51	48.59	0.80	17.54	7.21	0.236	6.67	11.45	2.57	0.34	0.12	0.05	4.73	100.30												1.08
G9608/52	53.55	0.85	17.87	9.48	0.170	4.22	9.87	2.15	0.18	0.10	0.01	1.76	100.21												2.25
G9608/55	52.43	0.65	18.18	8.97	0.178	5.73	10.99	2.49	0.56	0.12	0.02	0.00	100.31	597	66	22	286	280	109	96	18	10	42		1.57
G9608/58	59.05	0.82	15.91	7.29	0.170	2.79	6.14	3.63	1.15	0.13	0.01	3.02	100.11	257	29		209	190	109	139	11	20	27		2.61
G9609/01														154	63	30	227	295	127	164	33	37	42		
G9609/02	48.26	2.17	15.80	11.01	0.19	5.78	11.49	3.30	0.41	0.29	0.02	1.20	99.92	152	57	26	293	311	139	127	32	43	42		1.90
G9609/03	51.39	0.74	19.48	9.45	0.190	5.18	11.34	2.13	0.37	0.08	0.01	0.00	100.36												1.82
G9609/05	51.95	0.75	16.08	10.60	0.211	6.25	11.12	2.03	0.35	0.07	0.02	0.00	99.43	467	134	14	137	342	106	87	24	10	52		1.70
G9609/05	52.47	0.76	16.64	10.21	0.22	6.01	10.64	1.60	0.27	0.07	0.01	0.00	98.89												1.70
G9609/11	48.60	0.70	17.71	9.68	0.21	6.93	12.14	1.17	0.30	0.09	0.01	1.50	99.05												1.40
G9609/12	66.07	0.66	14.21	6.88	0.176	1.53	4.60	4.07	0.78	0.14	0.01	0.20	99.32												4.50
G9609/12	48.70	2.06	15.05	10.51	0.19	6.29	11.76	2.85	0.44	0.55	0.02	1.15	99.57							100				1.9	1.67

Table 8. Continued

Sample no.	SiO_2	TiO_2	Al_2O_3	FeO	MnO	MgO	CaO	Na_2O	K_2O	P_2O_5	Cr_2O_3	LOI	Total	Cr	Cu	Ni	Sr	V	Zn	Zr	Co	Y	Sc	Nb	FeO^*/MgO
G9609/13														819	112	6	169	299	100	93	20	10	39		
G9609/18	51.52	0.75	19.52	9.45	0.196	5.25	11.20	2.06	0.22	0.07	0.01	0.00	100.24							20				1	1.80
G9610/01	50.25	1.82	15.29	8.91	0.15	6.51	11.28	3.05	0.27	0.16	0.00	1.10	98.81	152	69	44	223	279	97	154	35	27	39		1.37
G9610/02														266	79	80	138	297	93	87	40	30	44		
G9610/08	47.12	2.41	17.71	9.66	0.15	5.88	10.02	3.38	1.22	0.81	0.02	0.95	99.34												1.64
G9610/12	49.61	1.39	15.40	8.82	0.17	7.47	12.14	2.66	0.27	0.10	0.03	1.10	99.16												1.18
G9610/16	47.08	2.52	18.77	10.08	0.15	2.46	10.59	3.63	1.31	0.88	0.03	2.20	99.69	175	53	65	581	245	131	200	28	31	25	24	4.10
G9610/18														171	50	107	522	200	123	214	33	32	25		
G9610/21	46.97	2.34	17.47	9.64	0.16	6.48	9.71	2.93	1.13	0.78	0.03	1.10	98.73	158	43	112	503	174	112	233	31	28	20		1.49
G9610/21a	47.74	2.28	17.47	10.21	0.15	6.75	10.31	1.74	1.16	0.81	0.02	1.10	99.75												1.51
G9610/25	47.26	2.54	18.52	10.05	0.16	2.99	10.34	3.82	1.38	0.90	0.03	1.80	99.78	166	56	67	586	253	125	256	30	35	28		3.36
G9610/30	47.63	2.50	17.84	10.21	0.18	3.68	10.21	3.82	1.15	0.81	0.03	1.65	99.71	189	80	58	460	244	142	250	32	35	27		2.77
G9610/31	47.61	2.35	18.08	9.39	0.16	3.77	10.73	3.34	1.09	0.68	0.03	1.95	99.18	210	64	68	578	233	121	225	31	32	27		2.49
G9611/01	50.00	3.00	14.38	11.30	0.20	5.09	9.60	3.89	0.73	0.38	0.01	0.15	98.72	40	63	28	311	275	124	230	28	40	33	26	2.22
G9611/02	51.12	3.26	14.16	11.50	0.21	4.04	8.77	4.70	1.00	0.48	0.01	0.10	99.35												2.85
G9611/03	49.98	3.03	14.74	11.37	0.21	5.23	9.72	3.75	0.78	0.39	0.01	0.00	99.21	32	60	26	297	282	126	230	33	40	33		2.17
G9611/04	50.37	3.06	14.41	11.49	0.20	5.20	9.47	3.98	0.90	0.41	0.01		99.49												2.21
G9611/12														30	49	15	267	266	132	286	24	45	29		
G9611/14														34	63	26	355	282	139	238	30	40	33		
G9612/02	54.52	2.58	14.02	11.25	0.24	2.81	6.23	5.26	1.40	0.57	0.01	0.10	98.98	17	29	7	230	146	171	480	18	74	24	41	4.00
G9612/04														12	28	4	226	148	166	566	18	72	23		
G9612/06	54.14	2.52	13.93	11.11	0.23	2.79	6.16	5.86	1.54	0.59	0.01	0.50	99.40	29	30	12	233	145	185	522	19	77	24		3.98
G9612/08	55.04	2.52	14.17	11.06	0.23	2.74	6.12	5.28	1.55	0.58	0.01		99.30	18	28	7	215	135	165	532	19	75	23		4.04
G9612/10	54.89	2.54	14.00	11.12	0.23	2.71	6.13	5.22	1.46	0.61	0.01	0.00	98.93	27	28	8	231	136	171	541	19	79	24		4.10
G9612/16	54.67	2.58	14.11	11.14	0.23	2.78	6.20	5.14	1.55	0.59	0.01		98.99	2	26	1	22	143	165	522	20	75	23		4.01
G9612/19	49.87	2.16	16.34	9.84	0.17	5.55	10.91	3.25	0.60	0.27	0.02		98.98	72	32	29	254	198	86	170	24	25	26	16	1.77
G9612/20														30	28	13	300	143	203	600	19	86	25		
G9612/22	53.49	3.09	14.21	9.60	0.29	3.13	7.43	5.65	0.23	0.69	0.01	1.40	99.21	7	30	7	309	198	227	368	24	63	27		3.07
G9613/01	50.36	2.89	14.66	11.41	0.21	5.31	9.55	3.67	0.76	0.38	0.01	0.00	99.20	34	47	245	293	275	123	220	28	38	32	24	2.15
G9613/03	50.81	2.86	14.50	11.62	0.21	5.23	9.59	4.30	0.88	0.39	0.01	0.00	100.39												2.22
G9613/04	50.40	2.87	14.49	11.33	0.20	5.12	9.54	3.95	0.86	0.39	0.01	0.10	99.27	36	49	24	315	304	139	257	34	45	37		2.21
G9613/05	50.66	2.84	14.37	11.37	0.20	5.17	9.49	3.58	0.86	0.37	0.01	0.05	98.97	31	49	23	270	260	117	239	29	36	30		2.20
G9613/06	50.53	2.85	14.35	11.47	0.20	5.17	9.50	3.61	0.83	0.37	0.01	0.00	98.90												2.22
G9613/07	50.65	2.84	14.41	11.30	0.21	5.15	9.42	3.76	0.85	0.38	0.01	0.05	99.03	33	49	25	284	263	117	277	27	37	31		2.19
G9613/13														35	47	25	280	292	138	260	33	41	33		
G9614/04	50.64	3.25	14.73	10.39	0.18	5.15	9.66	4.05	1.09	0.44	0.01	0.05	99.64												2.02
G9614/07	51.02	2.90	14.70	9.78	0.17	4.47	10.48	3.37	0.87	0.31	0.01	0.80	98.87	57	45	20	317	288	146	212	26	39	34		2.19

Table 8. Continued

Sample no.	SiO_2	TiO_2	Al_2O_3	FeO	MnO	MgO	CaO	Na_2O	K_2O	P_2O_5	Cr_2O_3	LOI	Total	Cr	Cu	Ni	Sr	V	Zn	Zr	Co	Y	Sc	Nb	FeO^*/MgO
G9614/10	49.61	2.07	15.75	9.19	0.15	6.41	12.41	1.76	0.69	0.29	0.03	1.05	99.40	259	60	59	322	242	91	161	26	27	36		1.43
G9614/14														43	44	25	340	316	131	315	26	38	33		
G9614/17	51.14	3.35	15.48	8.91	0.15	3.53	9.93	4.13	1.13	0.44	0.01	0.95	99.15	35	40	14	380	307	109	239	17	37	32		2.52
G9614/18	51.48	2.89	15.71	8.15	0.16	4.39	10.57	3.92	0.80	0.31	0.01	1.05	99.46	48	44	21	344	282	169	230	26	35	33		1.86
G9614/19	50.44	2.69	14.67	10.89	0.19	5.64	10.06	3.44	0.69	0.30	0.01	0.05	99.07	51	44	30	297	271	119	187	31	33	31		1.93
G9614/20	50.24	3.43	14.47	10.83	0.17	3.91	9.18	4.03	1.09	0.45	0.01	1.30	99.11	13	50	16	347	339	146	301	30	41	33		2.77
G9614/21	49.74	3.35	14.62	10.52	0.18	4.76	9.25	4.05	0.84	0.35	0.01	1.50	99.18	14	44	71	331	333	134	220	45	38	34	24	2.21
G9614/22	50.31	0.70	16.92	8.87	0.18	8.38	11.84	1.53	0.36	0.06	0.02	0.25	99.44	175	106	42	149	280	81	29	34	15	44	1	1.06
G9614/29	50.46	1.26	16.10	9.18	0.18	7.30	11.30	2.16	0.50	0.13	0.02	0.80	99.38							75				5.5	1.26
G9614/30	49.73	2.59	13.56	12.17	0.19	5.05	9.05	4.00	1.04	0.31	0.01	1.80	99.50	41	77	24	329	269	126	200	29	32	33		2.41
G9614/32	50.50	3.05	14.02	11.02	0.17	4.36	8.55	4.50	1.14	0.37	0.01	2.25	99.94	21	67	18	354	297	159	330	26	35	31		2.53
G9615/01	50.20	2.46	15.28	10.53	0.20	5.77	10.37	3.48	0.74	0.31	0.02	0.10	99.46	48	46	28	346	264	154	190	34	35	34	19	1.82
G9615/03	49.99	2.50	15.12	10.73	0.19	5.63	10.41	3.65	0.71	0.30	0.01	0.05	99.30												1.91
G9615/04	50.46	2.53	14.94	10.69	0.20	5.75	10.30	3.35	0.61	0.32	0.01	0.00	99.16	56	48	30	288	269	112	218	33	35	34		1.86
G9615/06	49.95	2.55	15.25	10.48	0.19	5.77	10.24	3.75	0.76	0.31	0.01		99.27	54	52	29	304	266	116	211	32	35	34		1.82
G9615/07	49.77	2.57	14.90	10.83	0.20	5.48	10.54	3.36	0.74	0.13	0.01		98.71	63	54	33	291	275	121	119	34	36	35		1.98
G9615/08	50.31	2.54	15.00	10.64	0.19	5.64	10.25	3.48	0.61	0.32	0.01	0.00	98.98	61	54	32	316	282	122	223	31	35	36		1.89
G9615/13														58	50	29	286	256	111	273	30	33	33		
G9616/01	46.74	2.81	16.20	10.86	0.09	5.13	11.31	2.28	0.77	0.43	0.01	2.25	98.88												2.12
G9616/02	47.40	2.20	16.82	9.97	0.272	6.54	11.44	3.18	0.61	0.37	0.03	1.51	100.34												1.52
G9616/06	46.79	2.11	16.36	10.48	0.422	6.45	11.34	3.22	0.70	0.29	0.03	1.91	100.10	380	49	103	366	255	188	169	47	21	36		1.62
G9616/07	44.42	2.20	14.64	11.52	1.275	6.66	10.99	3.01	0.55	0.30	0.03	4.66	100.25												1.73
G9617/01	47.42	2.36	16.28	9.17	0.15	7.26	10.63	3.16	1.05	0.32	0.03	1.10	98.92							170				24	1.26
G9617/02	49.42	2.29	14.69	11.63	0.21	6.60	10.11	2.83	0.35	0.23	0.00	0.95	99.35	174	52	79	145	335	141	187	31	44	39		1.76
G9617/05	48.19	2.29	15.09	10.10	0.17	7.02	9.75	3.53	0.22	0.24	0.03	2.40	99.03	203	44	90	145	259	109	253	29	35	28		1.44
G9617/06	49.44	2.62	15.94	9.45	0.13	4.33	10.60	3.80	1.41	0.37	0.01	0.95	99.06	41	44	17	462	292	103	214	24	29	31		2.18
G9617/07	46.74	1.53	17.28	8.62	0.22	7.25	9.94	3.17	0.23	0.13	0.03	3.95	99.10	254	56	124	143	238	104	131	34	28	34		1.19
G9617/09	51.36	2.25	14.94	8.80	0.15	6.66	8.30	3.95	0.17	0.23	0.03	2.25	99.07												1.32
G9617/11	48.72	2.25	15.21	9.68	0.16	6.92	9.15	3.38	0.30	0.24	0.03	3.25	99.29												1.40
G9617/12	49.91	2.32	15.12	9.51	0.19	7.82	7.56	2.74	0.12	0.24	0.03	3.40	98.95	185	38	82	150	258	112	143	28	33	29		1.22
G9617/13	47.16	2.38	14.55	11.68	0.17	7.76	8.18	3.10	0.20	0.24	0.02	3.50	98.95	142	56	69	95	326	102	214	29	40	36		1.51
G9617/14	48.67	2.15	14.70	7.71	0.16	6.58	9.22	3.48	0.24	0.26	0.03	3.60	99.00												1.17
G9617/16	51.65	2.31	14.87	9.37	0.169	7.06	7.63	3.13	0.22	0.27	0.03	3.54	100.25							160				13	1.33
G9619/01A	48.60	1.46	16.88	9.34	0.170	6.52	12.28	2.29	0.43	0.13	0.03	0.68	98.81							90				4.9	1.43
G9619/01C	49.49	1.63	15.10	10.64	0.184	7.09	11.99	2.40	0.43	0.15	0.03	1.32	100.46												1.50
G9619/02	50.61	0.83	15.45	10.24	0.188	8.13	11.08	2.02	0.40	0.07	0.03	0.00	99.05							38				1	1.26
G9619/05	49.14	0.62	17.49	9.10	0.165	6.65	12.99	2.03	0.42	0.07	0.01	1.44	100.13												1.37

Table 8. Continued

Sample no.	SiO_2	TiO_2	Al_2O_3	FeO	MnO	MgO	CaO	Na_2O	K_2O	P_2O_5	Cr_2O_3	LOI	Total	Cr	Cu	Ni	Sr	V	Zn	Zr	Co	Y	Sc	Nb	FeO^*/MgO
G9619/10	54.59	1.17	14.84	12.52	0.228	4.46	9.10	2.84	0.44	0.10	0.01	0.00	100.30												2.81
G9619/16	48.93	1.55	17.75	9.54	0.18	6.36	12.21	2.42	0.36	0.14	0.03	0.70	100.17												1.50
G9620/01	50.33	1.52	15.79	8.81	0.160	6.71	12.45	2.78	0.53	0.14	0.04	0.93	100.19							92				5.9	1.31
G9620/04	49.95	1.47	15.30	8.82	0.166	7.12	13.08	2.61	0.38	0.12	0.03	1.39	100.44												1.24
G9620/06	49.77	1.48	15.75	8.78	0.172	7.12	12.28	2.93	0.48	0.14	0.04	0.65	99.59							96				5.3	1.23
G9620/08	49.72	1.64	16.17	8.24	0.16	6.93	11.96	2.89	0.49	0.14	0.03	0.60	98.97												1.19
G9620/09	50.72	1.50	16.94	8.11	0.17	6.92	12.01	3.15	0.42	0.14	0.03	0.30	100.41	278	86	67	178	273	87	117	43	29	39		1.17
G9620/10	50.05	1.53	15.68	9.54	0.177	6.26	12.71	3.01	0.42	0.15	0.03	0.85	100.41												1.52
G9620/11	50.17	1.36	15.47	9.13	0.17	6.61	12.31	2.87	0.23	0.11	0.03	0.70	99.17	216	92	33	115	274	93	106	33	25	34		1.38
G9620/12	50.18	1.57	15.86	8.72	0.17	6.63	11.88	2.75	0.33	0.12	0.03	0.65	98.89	271	79	56	160	297	92	112	39	30	42		1.32
G9620/18														278	79	71	188	260	90	128	35	26	33		
G9620/23	63.00	0.93	14.27	7.02	0.20	1.68	4.85	5.36	1.94	0.19	0.01	0.90	100.35	15	95	23	169	178	152	156	17	33	24		4.18
G9621/01	56.69	0.82	15.83	10.00	0.203	4.18	8.34	2.79	0.79	0.11	0.01	0.00	99.76							67				1	2.39
G9621/04	49.94	0.70	18.98	9.67	0.19	5.76	11.41	2.26	0.30	0.07	0.01	0.00	99.30	21	229	18	161	306	88	78	34	15	42		1.68
G9621/06	51.39	2.94	13.76	10.46	0.198	5.34	10.67	3.06	0.56	0.30	0.01	0.84	99.53												1.96
G9621/07	48.79	2.47	13.54	14.07	0.225	5.96	10.47	2.97	0.35	0.24	0.01	0.72	99.81							150				9.3	2.36
G9621/10	47.88	2.95	14.07	13.18	0.23	5.41	10.09	3.10	0.47	0.32	0.01	1.35	99.08	52	64	23	159	431	182	195	33	56	45		2.44
G9621/12	47.67	2.95	12.53	15.74	0.28	5.91	10.69	1.40	0.43	0.29	0.00	1.10	98.99												2.66
G9622/01	46.92	3.89	16.73	11.51	0.17	4.57	7.44	3.88	1.68	0.60	0.01	1.30	98.70												2.52
G9622/02	47.34	3.81	16.40	12.26	0.167	4.84	7.79	4.28	1.74	0.62	0.00	0.97	100.22							340				40	2.53
G9622/03	47.40	3.81	16.36	12.37	0.172	5.00	7.79	4.22	1.76	0.64	0.01	0.79	100.32							330				40	2.47
G9622/06	49.12	0.88	18.39	10.37	0.195	5.68	11.77	2.18	0.28	0.07	0.02	1.44	100.39	631	155	66	166	413	129	81	21	9	43		1.83
G9624/01	50.27	2.10	14.86	11.48	0.199	6.91	10.87	2.92	0.44	0.23	0.02	0.00	100.30												1.66
G9624/02	49.81	2.17	14.49	11.23	0.193	6.27	10.87	3.16	0.57	0.22	0.02	0.16	99.16												1.79
G9624/03	49.94	2.25	14.84	10.92	0.20	6.41	10.69	2.76	0.50	0.22	0.02	0.10	98.85	130	50	67	138	356	114	189	35	43	40		1.70
G9624/05														143	65	76	136	347	118	149	36	41	40		
G9624/08	50.43	2.20	15.19	11.16	0.21	6.49	10.48	2.97	0.50	0.24	0.02	0.10	99.99	146	51	69	139	356	122	215	36	45	40		1.72
G9624/09	50.00	2.20	14.80	10.92	0.20	6.59	10.53	2.91	0.51	0.24	0.02	0.10	99.03	134	51	73	144	347	123	187	36	42	38		1.66
G9624/15	50.53	2.08	15.24	10.60	0.20	7.05	10.71	3.13	0.46	0.20	0.02	0.00	100.22												1.50
G9625/01	48.46	1.13	16.02	9.47	0.161	11.28	10.95	2.45	0.25	0.08	0.06	0.00	100.31							59				1.5	0.84
G9625/01	47.77	1.21	16.61	9.07	0.17	11.33	10.52	1.94	0.05	0.05	0.06	0.00	98.78												0.80
G9625/04														807	82	255	175	198	146	73	32	13	32		

Note: Analyzed by X-ray fluorescence at Central Analytical Laboratory. Vernadsky Institute of Geochemistry and Analytical Chemistry (GEOKhI). and at Geological Institute. Russian Academy of Sciences.

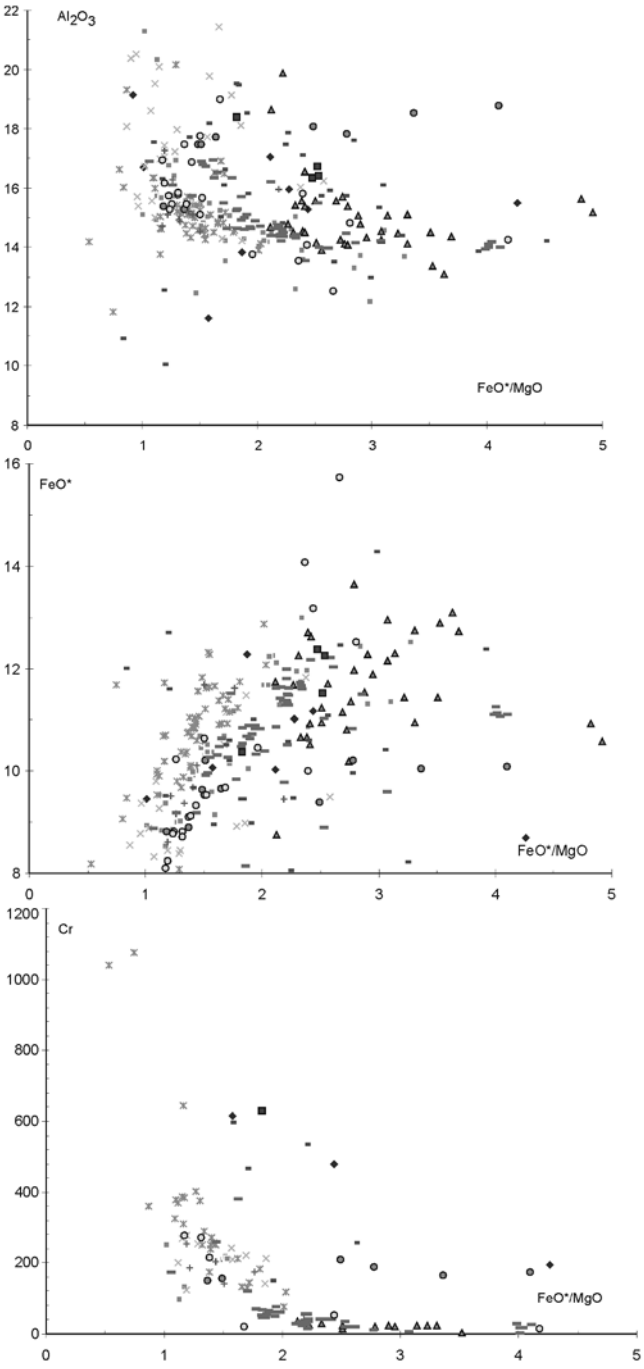

Figure 4. Al_2O_3, FeO*, and Cr vs. FeO*/MgO plots. For symbols, see Figure 2.

Basalts from the *rift zone of the Southwest Indian Ridge* are much less fractionated (FeO*/MgO = 0.7–1.5) than the Bouvet I. volcanics, and they do not go beyond the compositional range of basalts proper [*Didenko et al.,* 1999; *Le Roex et al.,* 1983; *Simonov et al.,* 2000]). At the same time, they display an extreme compositional diversity. The collection under study falls into four groups. A small group of samples are close in chemistry to the Bouvet I. hawaiites, and in the variation diagrams (Figures 2–4) they plot along the corresponding variation trends for the Bouvet I. volcanic suite.

In these diagrams, most basalts comprise a group that plots along independent short trends. Without attaining high degrees of differentiation, these basalts show a more rapid increase in K_2O and P_2O_5 than the Bouvet I. hawaiites, with the greatest K_2O abundances for a given fractionation index among the entire range of basalts from the Bouvet TJ region. This group is also generally lower in CaO and alumina and higher in TiO_2, whereas in terms of Na_2O abundances and variation patterns, the contents of lithophile trace elements such as Rb, Th, Nb, and Ta [*Simonov et al.,* 2000], and $(La/Sm)_n = 1.8–2.3$ and $(Nb/Zr)_n = 1.0–1.6$, they resemble the Spiess Ridge volcanics. At the same time, their considerably greater Cr and Ni concentrations are in a sharp contrast to both the Bouvet I. and Spiess Ridge basalts.

A minor group of basalts, noticeably lower in TiO_2, K_2O, P_2O_5, form no trend of their own due to a lack of systematic compositional variations. Their closest equivalents are enriched T-MORB-like tholeiites.

Their anomalously high K_2O (up to 3.35%) contents in certain samples from St. S1824, S1825, and S1835, combined with low FeO*/MgO values, are due to strong secondary alterations.

The Shona Seamount, judging from dredging data, is composed of various types of volcanics (Table 8). The most widespread rock type exhibits very low TiO_2 values, 0.6–1.2%. Taken together, these rocks make up a gently sloping, extensive differentiation trend from basalt (G9608/25, 27, 51, 55, G9609/3, 5, 11) to andesite (G9608/5, 13, 24, 29, 31, 37, 45) to dacite (G9608/28, 43, 58) through to rhyolite (G9608/8, G9609/12). This trend is sharply dissimilar to those for the Spiess Ridge and Bouvet I. volcanics. With increasing differentiation index, SiO_2 increases rapidly, while a very slow growth of TiO_2 (up to 1.2%), K_2O (up to 0.5%), and P_2O_5 (up to 0.15%) takes place, their overall abundances remaining low. In this group the basalts proper, as compared to the Spiess Ridge basalts, are incommensurably higher in Cr (ca. 500 ppm), higher in V and Sc, noticeably lower in lithophile elements Sr, Zr, Y, Nb, and have similar Ni abundances. With progressive differentiation, Cr, V, and Sc decrease rapidly, while Sr, Zr, Y, and Nb, in contrast, show a gradual growth. These volcanics are characterized by low $(Nb/Zr)_n$ ratios in the range 0.1–0.5. The dominant varieties are strongly vesicular scoria, volcanic bombs, and pumice, although the common moderately to weakly vesicular rocks are present as well. Most of the rocks are fresh, and some are strongly oxidized.

The rest of the Shona Smt. volcanics are solely represented by basalts, classifiable into several minor groups. Sample G9608/15, strongly vesicular, is chemically similar to the Spiess Ridge basalts, but very high in Cr (535 ppm), a feature rendering it more close to the SWIR rift-valley basalts. Two samples (G9608/45, 52) are close to depleted tholeiites. They also show characteristically low TiO_2 and even lower K_2O contents than the main rock group from the Shona Smt. The slightly enriched tholeiitic varieties include basalts G9608/4 and G9609/2, distinguished from the two preceding groups by higher K_2O (0.40%) and TiO_2 con-

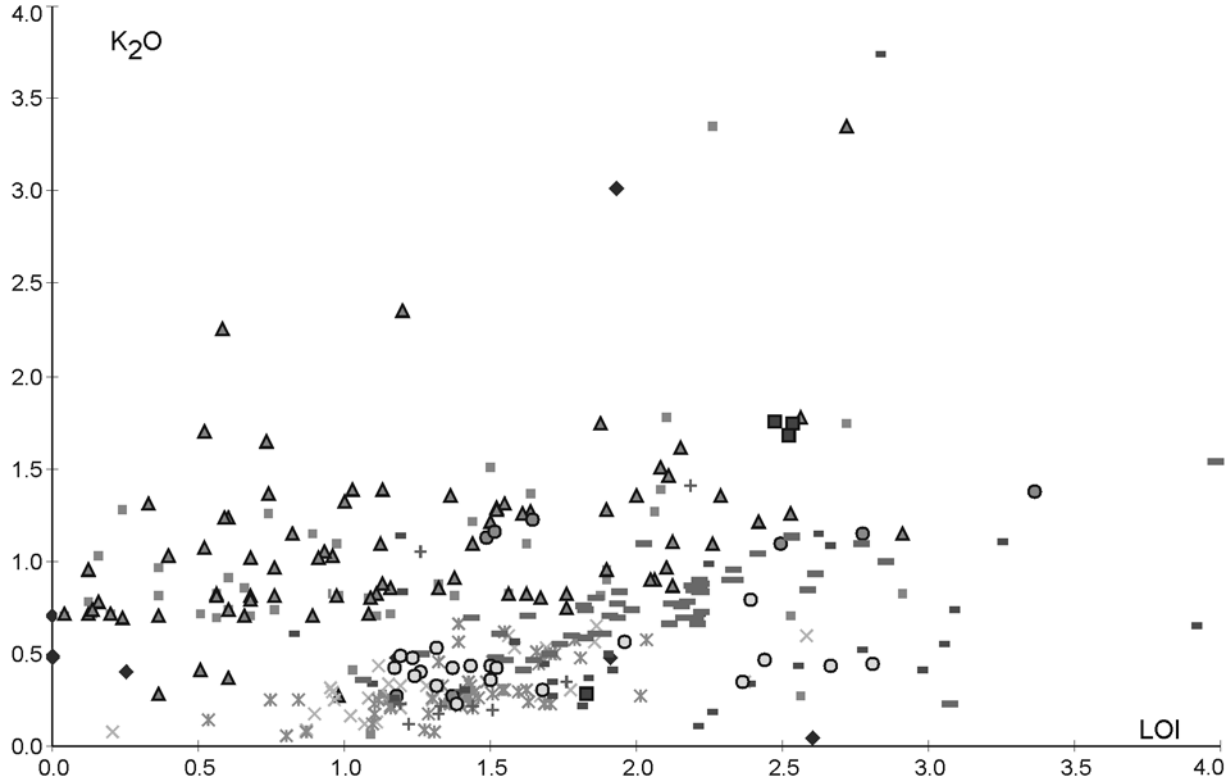

Figure 5. K_2O vs. LOI (loss on ignition) plot. For symbols, see Figure 2.

tents. Two uncommon basaltic compositions (G9608/3, 46) have been encountered. The former is essentially Ol-phyric, a circumstance reflected in its low silica and alumina and high Cr and Ni contents. In the contents and proportion of potassium and phosphorus, it resembles the enriched basalts from St. G9610. In terms of these parameters, the altered samples, G9608/24 and 46, are also close to basalts from this station. Note that all the basalts that differ from the main group of Shona Smt. volcanics are virtually non-vesicular, part of them being noticeably altered, and some show evidence of having been broken off the slope.

From the *linear high,* which extends from the southern part of the Spiess Ridge toward Bouvet I. and apparently provides a structural link between the two, several basalts of essentially distinctive compositions have been dredged (St. G9622). Most of the samples are strongly evolved, high-Fe ($FeO^*/MgO = 2.5$) basalts enriched in TiO_2 (3.8–3.9%), K_2O (1.7–1.8%), P_2O_5 (0.6%), and Na_2O (3.9–4.3%) (Table 8). Their $(Nb/Zr)_n$ ratio is 1.3. Based on these and other parameters, these basalts, as appears from their variation plots (Figures 2–4), are strongly similar to those rocks from the Southwest Indian Ridge rift valley that are distinguished by high K_2O and P_2O_5 contents. Remarkably, Smp. G9622/2 is very high in Cr.

The one exception is Smp. G9622/6, which otherwise, for either the character of its secondary alteration or structure, does not stand out among this group. It is low in TiO_2 (0.88%), Na_2O (2.18%), K_2O (0.28%), P_2O_5 (0.07%) and has $FeO^*/MgO = 1.8$, traits resembling the Shona Rise volcanics.

A distinctive feature of the volcanics dredged from the *walls of the Bouvet Fracture Zone* is their extreme petrographic and chemical diversity. Overall, these are weakly to moderately evolved rocks somewhat low in SiO_2 (44–46%) [*Simonov et al.*, 2000]. Their degree of secondary alteration (0.8 to 1.8% LOI) matches that for the MAR basalts. In the TiO_2 vs. FeO^*/MgO plot (Figure 2), these basalts follow two essentially distinct trends. The overwhelming majority plot on the MAR trend, with TiO_2 varying from 1.0% to 2.0%. They are typified by $(La/Sm)_n = 0.7–1.2$ and $(Nb/Zr)_n = 0.6–1$, values not falling outside the MAR basaltic range. The second group of basalts follows the Shona Smt. trend, in which TiO_2 contents do not exceed 1% for $FeO^*/MgO = 1.6–2.6$. The $(La/Sm)_n$ and $(Nb/Zr)_n$ ratios in a sample representing this group are 0.93 and 0.81, respectively.

Certain basalts from the Bouvet Fracture Zone are relatively abundant in plagioclase phenocrysts, which is reflected in their elevated CaO and Al_2O_3 contents.

Most part of the basalts from the *East Dislocation Zone* (Table 8), dredged at St. G9617, are characterized by low fractionation indices of 1.2–2.2 for high TiO_2 (averaging 2.3–2.4%). Low K_2O (0.1–0.3%) and P_2O_5 (0.1–0.25%) contents, $(La/Sm)_n = 1.2$, and $(Nb/Zr)_n = 0.7–0.9$ render these basalts similar to those from the MAR. All these basalts are noted for broadly developed chlorite and a number of other relatively high-temperature secondary minerals formed at el-

evated conditions, presumably deep in the basalt pile. This is reflected in their chemical composition: these basalts are typified by lowered CaO contents, and some show increased Na_2O abundances.

Samples G9617/01 and G9617/06 are exceptional in their considerably elevated K_2O (1.0–1.4%) and P_2O_5 (0.3–0.4%) abundances and $(La/Sm)_n$ = 2.5 and $(Nb/Zr)_n$ = 1.5–1.6. In this respect, they are close to the SWIR rift valley basalts but, in terms of their extremely low Cr contents, they match the Spiess Ridge and Bouvet I. basalts. They also differ from the main group in their type of secondary alteration, displaying only a minor amount of low-T alteration products.

Basalts from the *easternmost segment of the AAR* are classifiable into two groups. One is represented by as few as two samples, G9604/54 and G9602/03, with elevated TiO_2 (2.2–3.1%) and P_2O_5 (0.2–0.4%) contents at relatively low FeO^*/MgO, 1.6–1.9 (Table 8), with $(Nb/Zr)_n$ = 0.4–0.6 and $(La/Sm)_n$ = 0.9–2.1. These rocks are generally close to the slightly enriched basalts from the southern terminus of the MAR. They show a relatively extensive development of chlorite. The main group of basalts exhibits various degrees of differentiation (FeO^*/MgO = 1.0–2.4), with very low TiO_2 contents (0.8–1%), 0.4–0.53% K_2O, 0.08–0.09% P_2O_5, and $(Nb/Zr)_n$ = 0.3. These compositions plot along the Shona Smt. differentiation trend. More silicic varieties, with 62% SiO_2, also falling on this trend, have been encountered in this group. It should be noted that these basalts are overall less altered or even fresh. They vary in aspect from nonvesicular to strongly vesicular, resembling volcanic bombs.

Basalts dredged from the *rise between the two troughs into which the south tip of the MAR bifurcates* (St. G9610) are moderately to strongly evolved, with FeO^*/MgO ranging from 1.2 to 4 (Table 8). These are classed into two groups. One group (G9610/1, G9610/12) is low in lithophile elements (0.3% K_2O, 0.1–0.2% P_2O_5) and has low $(Nb/Zr)_n$ ratios, corresponding to N-MORB from the MAR. The other group is considerably higher in K_2O (1.1–1.4%) and P_2O_5 (0.7–0.9%) and has elevated $(Nb/Zr)_n$ = 1.32, with Smps. G9610/8, G9610/21, G9610/31, for a low fractionation degree, showing anomalously high P_2O_5 (0.7–0.8%) and Sr (500–600 ppm) abundances. Another peculiarity of these rocks is the narrow range of TiO_2, Al_2O_3, and CaO contents through differentiation. In the variation plots, the enriched basalts form trends of their own, not corresponding to those for the Spiess Ridge and Bouvet I. In terms of Sr, Rb, and Ba abundances they plot in the arrays of basalts from the 12–14°E anomaly [*Le Roex et al.*, 1992], but have distinctly lower Y and Nb contents. The two basalt groups differ in terms of secondary alterations as well. The first is almost fresh, with a minor amount of glauconite, and the second contains smectite, pointing to its deeper position in the basaltic stratigraphy.

The zone in which the America-Antarctic, Southwest Indian, and Mid-Atlantic ridges converge (St. G9619, G9620, and G9621) yielded volcanites of three geochemical types (Table 8). Type 1 comprises weakly evolved basalts of N-MORB affinity, fitting in with the compositional range of MAR basalts at the Bouvet TJ (FeO^*/MgO = 1–1.5, 0.2–0.3% K_2O, 0.07–0.15% P_2O_5, 1.4–1.6% TiO_2, $(Nb/Zr)_n$ = 0.5–0.7). Type 2 is distinguished by elevated contents of lithophile elements (K_2O and P_2O_5) and TiO_2 (2.5–3.0%), characteristic of slightly enriched tholeiites, while showing relatively low $(Nb/Zr)_n$ ratios. Some of these basalts are noted for very high Cr contents, 500–800 ppm. Type 3 (G9619/2, 5, 10, G9620/23 and G9621/1, 4), low in TiO_2 (0.6–1.2%) and P_2O_5 (0.07–0.1%), also has low $(Nb/Zr)_n$ ratios, 0.2–0.3. Among this type one finds strongly differentiated varieties, dacite inclusive. Chemically similar volcanites are widespread at the Shona Smt. We analyzed, for the most part, slightly altered samples, but rocks representing Type 3 are distinguished from Type 1 and 2 basalts in being more strongly vesicular.

Principal geochemical groups of basalts: Spatial distribution and geodynamic settings

The above section shows the Bouvet TJ to be an area of distribution of highly diverse volcanites, with basalts as a dominant variety. In classifying and grouping these rocks, we proceeded from the following premises. Elements that communicate the fingerprints of the mantle source of primary melts are Ti, P, K, and some other incompatible elements (Nb, Zr, Y), whose ratios change only slightly in partial melting and melt fractionation processes. For this reason, the abundances and ratios of these elements are the main criteria whereby to subdivide volcanics into groups. At the same time, in view of considerable potassium mobility in seafloor weathering of basalts, we discarded rocks with high water contents in classifying the rocks into groups; and the behavior of P and Ti at very high differentiation degrees is controlled by co-precipitation of apatite and Fe-Ti phases. The latter circumstance also bears on the distribution of incompatible elements such as Nb, Zr, and Y. Among the parameters of critical importance to mantle source characterization are isotope ratios and rare earth element (REE) distribution patterns in volcanites. We have made no contribution of our own along this line of study, but in a number of cases published data are available for one or another rock group.

As regards the other elements, their variations are largely controlled by the character of magma differentiation, which gives rise to evolved volcanic suites, identifiable mainly through the analysis of variation diagrams for elemental abundances versus the fractionation index, FeO^*/MgO. In these diagrams, the volcanic suites form trends that either are roughly parallel, suggesting closely similar fractionation conditions, or intersect. The availability of discrete trends portraying the behavior of individual elements might either point to mantle source inhomogeneities or to distinctions in partial melting conditions for particular rock groups. Thus, *Klein and Langmuir* [1987] deduced from a study in basaltic glasses that elevated Na contents of primary melts indicate lower degrees of partial melting in the mantle source region, whereas elevated Fe contents point to greater magma generation depths.

It is worthwhile to note that diverse volcanic suites or

groups may produce identical trends in some diagrams but distinct trends in others, which hampers an unequivocal identification of the suites. Besides, basalts generated from chemically distinct magma sources may yield similar fractionation trends for particular elements.

The most common and widespread basalt group at the Bouvet TJ is N-MORB, whose prime hallmark is its low lithophile element content. The rocks are weakly to moderately evolved and, rather than forming an extensive trend, they plot in compact clusters in variation diagrams, at the source of all the differentiation trends. Only in the FeO^* vs. FeO^*/MgO diagram (Figure 4), do basalts from this group make up an independent trend with the highest FeO^* abundances. Previous studies [*Simonov et al.,* 1996, 2000] showed these basalts to be likely derivatives of partial melts separated from the mantle beneath mid-oceanic ridges starting at 60- to 70-km depths. In the study region, they are most widespread within the MAR rift valley and flanks. In the other two spreading ridges, SWIR and AAR, they are encountered less frequently (within Bouvet Fracture Zone and Conrad corner high), although according to *Le Roex et al.* [1983, 1985], outside the Bouvet TJ such rocks are widespread on these ridges as well. Depleted basalts have also been recovered from the junction zone of the MAR and SWIR fossil structures, or East Dislocation Zone. In that area, the rocks are strongly altered, the dominant secondary mineral being chlorite, which is consistent with their exhumation on the seafloor surface from deeper levels in the oceanic crustal stratigraphy. In the junction zone of the MAR, SWIR, and AAR, this basaltic group makes up a number of highs, but in this case they bear evidence of a merely superficial alteration. Sporadic N-MORBs were dredged from the lower part of the Shona Rise. N-MORBs are thus ubiquitous in the Bouvet TJ region. A number of elements, especially Na and Ti, show within group variability not correlatable to any spatial distribution pattern for the varieties thus discriminated. Basalts from the East Dislocation Zone are noted for their lower CaO contents due to extensive development of chlorite. In contrast, certain essentially Pl-phyric varieties at the Bouvet Fracture Zone are typified by elevated CaO and, particularly, Al_2O_3 contents.

The group just mentioned is closely similar in chemistry to moderately enriched tholeiites, T-MORB. They differ from the depleted varieties by being higher in lithophile elements K, P, Zr, Sr, Y, Nb, etc., whose degree of enrichment is variable. These rocks also display greater incompatible element ratios, Nb/Zr, La/Sm, etc. T-MORBs have been encountered at virtually all the localities from which depleted basalts were described, although in smaller amounts. Sporadic T-MORB samples were found on the Spiess Ridge as well.

Volcanics dredged from the Spiess Ridge and Bouvet I. submarine slopes in the TiO_2, K_2O, P_2O_5 vs. FeO^*/MgO plots (Figures 2–4) jointly form a continuous, independent, extensive trend, reflecting a protracted differentiation that involved enrichment in Fe, Na, and K and depletion in Mg, Ca, and Al. Judging from the shape of the trend, Fe, Ti, and P increased rapidly through initial fractionation stages, whereas at the final stages, as Fe-Ti phases (ilmenite?) and apatite precipitated in an intermediate magma chamber, their abundance in the melt dropped considerably. Despite such an extensive differentiation trend, silica content increased only slightly prior to the onset of precipitation of apatite and Fe-Ti phases. Such a differentiation pattern is intrinsic in tholeiitic melts that follow the Fenner trend. Among the Bouvet I. volcanites, strongly evolved varieties are considerably more common than on the Spiess Ridge, suggesting much greater dimensions for the intermediate magma chamber beneath the Bouvet volcano. This is further supported by the Bouvet I. volcanic edifice being much greater in plan size.

Although we have assembled the Bouvet I. and Spiess Ridge volcanics into a single suite, there are some distinctions between them. In the Na_2O, Al_2O_3, and FeO^* vs. FeO^*/MgO diagrams, they form discrete parallel trends, with Na_2O and FeO^* being higher and Al_2O_3 lower in the Spiess volcanics for equivalent FeO^*/MgO values. This distinction implies different primary melt generation conditions for the Spiess Ridge and Bouvet I.

In the variation diagrams portraying the behavior of trace elements, the Bouvet I. volcanics show greater Nb/Zr and Zr/Y ratios cf. the Spiess Ridge. This distinction might be due either to mantle-source inhomogeneities or crystal fractionation processes, considering that our analysis focused on strongly evolved rocks in the first place. Certain differences between the Bouvet and Spiess volcanics follow from isotopic data as well [*Kurz et al.,* 1998; *Sushchevskaya et al.,* 1999]. The Bouvet I. volcanics exhibit rather high abundances of radiogenic Sr and Pb isotopes ($^{87}Sr/^{86}Sr$ = 0.70371, $^{206}Pb/^{204}Pb$ = 19.588), rendering them sharply dissimilar to the depleted basalts, in particular, from the south end of the MAR, with 0.70323–0.70338 and 18.037–18.932, respectively. The Spiess Ridge volcanics display generally low $^{87}Sr/^{86}Sr$ ratios (0.70329 to 0.70336), matching depleted MORB, although for certain basalts this ratio is greater, 0.70349, while $^{206}Pb/^{204}Pb$ ratios are transitional, 19.010 to 19.244. The Bouvet I. volcanics yielded high radiogenic He values, $^3He/^4He$ = 12.4, which decrease away from the island. Elevated radiogenic He values in Bouvet I. volcanics in conjunction with high radiogenic Sr and Pb isotope values indicate their primary melts to have been related to a deep-seated enriched mantle plume. On the other hand, the Spiess Ridge volcanics are marked by very low $^3He/^4He$ = 2.15–7.44, values generally even lower than the depleted MAR basalt range, 7.11 to 7.66 [*Kurz et al.,* 1998]. Therefore, proceeding from the existing notions on the genetic role of isotopic and geochemical indicators, one cannot put forward any internally consistent model to account for the genesis of the Spiess Ridge volcanic rocks. On the one hand, their K, P, Ti, and some trace lithophile element abundances are close to those in the Bouvet I. volcanites, whose plume affinity, as discussed above, is supported by extensive evidence. On the other hand, their isotope values are contrasting. The Sr isotope signature is close to depleted tholeiites, while Pb isotope characteristics are intermediate between depleted basalts and Bouvet I. volcanics, and radiogenic He values as low as that might be due to either dilution of their primary melt by a radiogenic He-enriched component or an early degassing event in the mantle source region. *Sushchevskaya and co-workers* [1999] hypothesized,

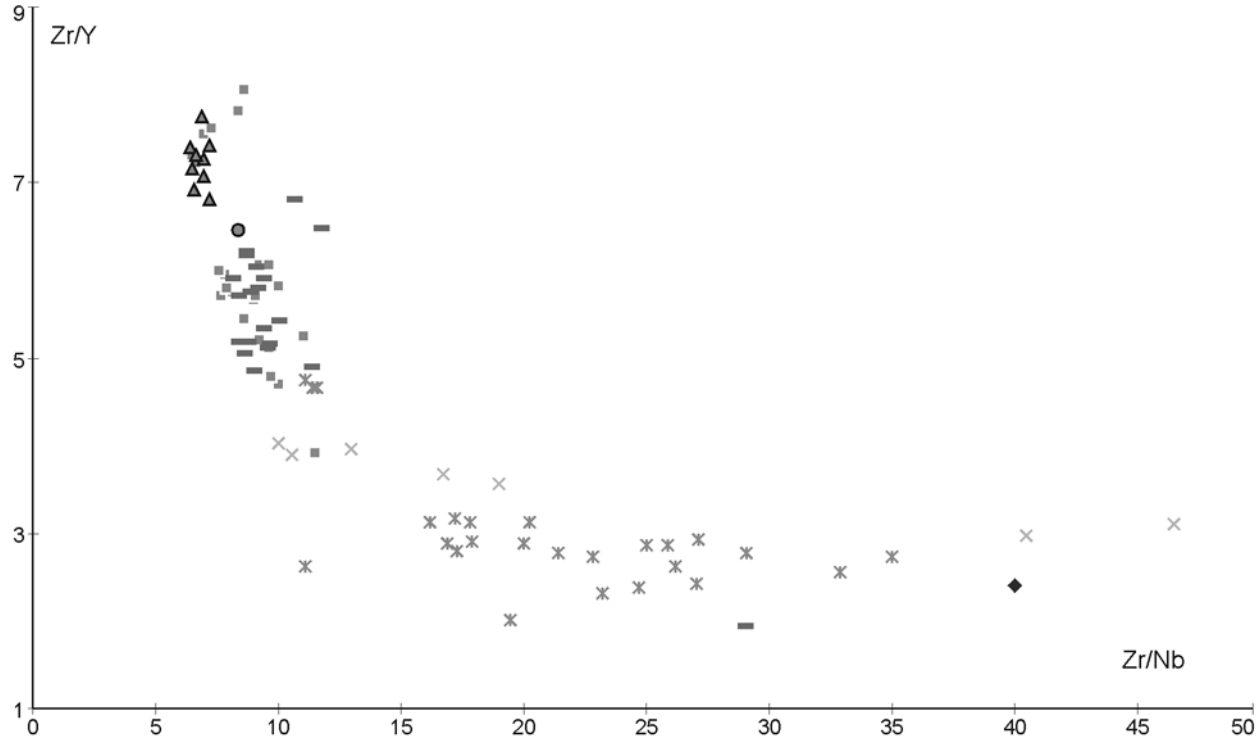

Figure 6. Zr/Y vs. Zr/Nb plot. For symbols, see Figure 2.

interestingly, the Spiess Ridge volcanics to have originated through the melting of a metasomatized mantle formed at an earlier rifting stage. That such a mantle may have survived in the modern axial parts of the spreading ridges follows from the complex geodynamic scenario for the opening of this part of the Southern Ocean. Postulating metasomatized mantle as a magma source would account for the certain amount of radiogenic isotope enrichment and low radiogenic He values for the Spiess Ridge volcanics. Although the inference of a metasomatized mantle occurring in this region provokes no objections, there still is a number of observations, primarily geological, that prevent one from accepting this viewpoint unreservedly. The Spiess Ridge began to form at ca. 2 to 2.5 Ma, and the Spiess volcano proper, at ca. 1 Ma, when the end segment of the SWIR already existed, having had formed at ca. 10 Ma [*Ligi et al.,* 1999]. At the early stages of existence of this segment, basalts erupting along its axial zone were for the most part depleted, as evidenced by basalt chemistry data from St. G9620 and G9621, located on the west flank of this segment.

The Spiess Ridge and Bouvet I. volcanics have some structural features in common. Both make up major rises crowned by central-type volcanic edifices underlain by large intermediate magma chambers. These volcanic edifices began to form roughly synchronously. Calling up this additional evidence, we nonetheless favor the idea that the mantle source for the Spiess Ridge primary melts was provided by the same plume that produced the Bouvet I. melts. This plume is rising to the surface via two principal channels that merge at depth. Because the channel located beneath the Spiess Ridge is juxtaposed with the spreading center, enriched melts are mixing with depleted ones, typical of oceanic rift volcanism. The plausibility of plume-derived melts mixing with depleted N-MORBs follows from the Zr/Y vs. Zr/Nb diagram (Figure 6). It suggests that not only Spiess Ridge basalts result through the mixing of the above end members in various proportions, but so do the enriched basalts from the MAR and SWIR rift valleys. Obviously enough, however, the mixing processes are very complex and cannot in full be accounted for by the overly simplified model of *Shilling et al.* [1985]. Indeed, in the Spiess Ridge volcanics the contents of some elements (K, Ti, P, Cr, etc.) match those in the plume melts (Bouvet I. volcanics), while other features such as the ratios of incompatible trace elements and Pb isotopes have intermediate values and, lastly, Sr and He isotope ratios are close to those from depleted melts. The enriched tholeiites from the MAR rift valley, also shown above to be likely mixing products of plume-derived and depleted melts, display other relations of their components. In particular, they differ from the Spiess Ridge volcanites in having lower contents of incompatible lithophile elements and Na, but noticeably greater Mg, Cr, V, and Sc contents. The interplay of the plume source and depleted basalt source is not restricted to the mixing of their respective melts. The higher Na_2O and FeO^* contents of the Spiess Ridge volcanics as compared to Bouvet I. suggest their partial melting conditions to have been dissimilar as well. Not inconceivably, it is due to changes in these conditions that metasomatized mantle, whose presence for this region is advocated by *Sushchevskaya et al.* [1999], became involved in melting, which would account for the low $^3He/^4He$ ratios of the Spiess Ridge volcanites.

Therefore, in view of the fact that Spiess Ridge and Bouvet I. volcanics form a continuous differentiation trend in the TiO_2, K_2O, and P_2O_5 vs. FeO^*/MgO diagrams, they can be somewhat arbitrarily viewed as jointly forming a coherent volcanic suite. The same trend is followed by some of the basalts from the SWIR rift valley.

However, a considerable part of basalts from the SWIR rift valley constitute an independent group. The main criterion for its discrimination is the fact that in the K_2O and P_2O_5 vs. FeO^*/MgO plots (Figures 2–4) these basalts form independent trends with greater K_2O and P_2O_5 contents cf. Bouvet I. volcanics for equivalent FeO^*/MgO values. The independence of this trend might as well be an artifact of understated FeO^*/MgO values due to decreased FeO* or increased MgO contents of these basalts as compared to Bouvet I. rocks. But they do not differ in terms of MgO, while FeO^*, on the contrary, is higher in this group of basalts, hence the elevated P_2O_5 and K_2O contents are signatures of their primary melts. Another critically important distinction of these basalts from the Bouvet I. volcanics is their considerably greater Cr content. Indicator ratios of trace elements such as Nb/Zr and La/Sm in these rocks are close to those from the Spiess Ridge basalts. In general, isotope data for rift valley basalts from this SWIR segment [*Kurz et al.,* 1998] display relatively high values of radiogenic Sr ($^{87}Sr/^{86}Sr = 0.70322$ to 0.70378), Pb ($^{206}Pb/^{207}Pb = 19.287$ to 19.343) and He ($^3He/^4He = 8.1$ to 12.9), closely similar to those for the Bouvet I. basalts. It thus would be reasonable to attribute the petrogenesis of these basalts to the mixing of melts separated from a deep mantle plume head centered beneath Bouvet I. and from depleted mantle. This, however, would also require an explanation of how their primary melts became additionally enriched in K and P.

To elucidate the nature of these melts, it should be recalled that compositionally similar basalts were recovered not only from the SWIR rift valley, but also from the linear rise between the Spiess and Bouvet volcanoes and from the East Dislocation Zone, i.e., from within-plate structural features of a volcano-tectonic origin. Basalts encountered there and belonging to this group are not infrequently anomalously high in Cr. Our inferences in this context are as follows. From the two principal channels of the deep mantle plume located beneath the Bouvet and Spiess volcanoes, a fluid-enriched material is spreading along the underside of the lithosphere. Fluid-controlled differentiation of the mantle material in the upwelling plume might be evidenced by the high water content of the melts parental to Spiess Ridge and Bouvet I. volcanics [*Simonov et al,* 1996], these contents being essentially higher in the rift-valley basalts at Bouvet I. cf. Bouvet I. proper, for equivalent differentiation indices. Fluids, for which K and P have an especially strong affinity, additionally enrich the spreading plume material in these elements. The resultant plume derivatives may serve as magma sources, given favorable permeability conditions such as exist in rift valleys and zones of vigorous within-plate tectonism. As the fluid-rich melts thus formed interact with the upper mantle material, they become enriched in Cr. The restites contain abundant Cr-spinel which, according to *Seyler and Bonatti* [1997], is most susceptible to compositional changes in interacting with mafic melts. The Cr enrichment process is very irregular, as would be expected in view of the non-uniform spinel distribution in the restites.

A compositionally independent group is formed by the majority of basalts dredged from St. G9610, which sampled a rise at the south tip of the MAR. In the K_2O, TiO_2, and P_2O_5 vs. FeO^*/MgO diagrams, these share a common trend that crosses at an angle the trends of the other volcanic suites. This is a rather extensively differentiated basalt suite, showing essentially greater P_2O_5 contents than the other volcanite groups for equivalent FeO^*/MgO values. They are also characterized by rather high K_2O and trace lithophile element abundances, matching those from Bouvet I. and Spiess Ridge volcanic suites, with essentially greater abundances of such elements as Ce, Th, Ba, B, and Sr [*Sushchevskaya et al.,* 1999]. The differentiation trend for these basalts differs from the typical tholeiitic trends in that, with differentiation, K_2O, TiO_2, P_2O_5, and Al_2O_3 increase very slightly. Isotopic characteristics from basaltic glasses [*Sushchevskaya et al.,* 1999] (Smp. G9610/37) are in a sharp contrast to all the other volcanics from the vicinity of the Bouvet TJ and Bouvet I. The main distinctions lie in the anomalously high $^{87}Sr/^{86}Sr = 0.70545$ and in the high $^{208}Pb/^{204}Pb = 39.23$. Such features are characteristic of continental mantle material or ancient oceanic mantle. We assume these enriched basalts to compose deeper horizons in the stratigraphy of the rise because their secondary mineral is smectite and because they give way upward to depleted basalts containing only a superficial alteration product, glauconite. The enriched basalts thus portray an early formative stage of the rise, synchronous with the convergence at a point of the three spreading ridges, Mid-Atlantic, Southwest Indian, and America-Antarctic, at 1 m.y. BP [*Skolotnev,* 2000]. It can be inferred that, owing to these circumstances, the preexisting lithosphere was extremely hot. Presumably, the heating might have induced partial melting in a lithosphere that contained blocks of continental mantle or ancient oceanic crust, and the melted material was added to depleted N-MORB melts.

Needless to say, the issue of the provenance of blocks of a continental mantle or ancient oceanic crust near the axial parts of the mid-oceanic ridges is no less debatable than the nature of the basalts under study. In this context, the following is worth noting. The study region is very complex in terms of both the oceanic floor structure and geological history [*Dubinin et al.,* 1999; *Pushcharovsky,* 1998], and the AAR and SWIR are believed to have converged with the MAR relatively recently. Prior to that, this region had been the locus of other spreading centers, whose traces are discernible with confidence in the seafloor fabric. Obviously, such global rearrangements in the geodynamic setup of this region favor preservation of blocks of a continental mantle or ancient oceanic crust in the younger oceanic lithosphere.

Lastly, a compositionally independent group is comprised by the greater part of Shona Smt. volcanics. These form an extensively differentiated suite, whose trend differs sharply from those of the other volcanic groups. Firstly, the most primitive basaltic varieties in this group, as compared to their counterparts from the other groups, are extremely depleted in TiO_2 and low in P_2O_5. Secondly, with progressive differentiation the melt shows a very slow enrich-

ment in TiO_2, K_2O, P_2O_5, and FeO^*, while SiO_2, in contrast, increases very rapidly. The rocks are also low in K_2O, although generally they exceed in this parameter depleted N-MORBs. Taken together, these differentiation features are characteristic of calc-alkaline, rather than tholeiitic melts, and the former are commonly known to be widespread in suprasubduction-zone settings. Their further features in common with calc-alkaline magmas are the presence of orthopyroxene phenocrysts, elevated Fe-numbers of their olivine phenocrysts (Fo_{72-80}), and high-Ca plagioclase phenocrysts (An_{86-96}). The Shona Smt. volcanics, however, show essential distinctions from typical calc-alkaline volcanics. They are noticeably higher in MgO and CaO and somewhat lower in K_2O, Na_2O, and Al_2O_3, but the main distinction lies in their very high Cr content, an order of magnitude greater than in volcanic-arc basalts. A prime feature of island-arc volcanics is known to be the Nb-Ta trough in spidergrams. We had no opportunity to study in detail trace element patterns from the Shona Smt. volcanics, and it thus cannot be ascertained unequivocally whether this trough is present in them or not. Volcanics with such compositions are utterly unusual to the oceanic crust, which calls for weighty proofs of their in situ and not ice-rafted provenance, as this region is in the range of iceberg distribution.

We believe these rock samples to be autochthonous, as they bear no glacial striations, and the nearest source of island-arc material is South Sandwich Is., whose area is negligibly small, and where no icebergs proper are forming. Antarctica, in contrast, does supply ice-rafted material, but this material is characteristic of the continental crust and includes gneiss, granite, sandstone, etc., although calc-alkaline volcanics are known from that region as well. Yet more critical evidence for bedrock origin of this type of volcanites follows from the study of their structural characteristics. Alongside the dominant strongly vesicular varieties, odd in aspect indeed, but generally resembling the Spiess Ridge volcanics, this group includes non-vesicular rocks that differ in no way from the typical oceanic basalts. From the abraded top of the Conrad corner high, dacites that belong to this group have been recovered as constituents in a breccia with a sandy matrix. The matrix grains are composed of clasts of this particular type of volcanics.

As discussed above, in a number of features the Shona Smt. basalts are close to island-arc calc-alkaline suites, but their final identification requires a more detailed study of their trace-element and isotope composition. It is not unlikely that we are dealing with a mere coincidental resemblance. Nonetheless, we will venture to propose a number of inferences on the origin of this volcanic suite based on the current notions on the genesis of calc-alkaline rocks. Major efforts along this line of study have been centered on the search of a satisfactory explanation for the somewhat enriched character of their primary melts in light lithophile elements in conjunction with the Nb-Ta deficit. Assumedly, primary calc-alkaline melts are generated in the metasomatically pre-enriched suprasubduction mantle. The source of metasomatizing fluids is the oceanic slab, subducted to great depths. Some writers [*Ringwood,* 1990] attribute the low Ti, Nb, Ta, etc., concentrations to rutile crystallizing as a residual phase. Others invoke the fact that these elements are less mobile as compared to the other lithophiles [*McCulloch and Gamble,* 1991], postulating their source to be a pre-depleted mantle material. Further evolution of the melts and their differentiation conditions, resulting in calc-alkaline suites, are addressed in detail in [*Frolova et al.,* 1985]. T. I. Frolova invokes three conditions prerequisite for calc-alkaline suites to form: (i) vigorous fluid activity in the area in question, (ii) compressional regime favoring the formation of closed intermediate chambers ensuring melt differentiation in the presence of fluids and increasing silica enrichment and oxidation state of these fluids, and (iii) assimilation of mafic country rocks by the melt.

To elucidate the nature of the Shona Smt. volcanics, it should be kept in mind that similar rocks have locally been encountered at the junction zones of the fossil structures of the SWIR and AAR, as well as of the AAR and MAR, in which these rocks are involved along with depleted basalts in complex tectonic structures. Note that, judging from their more fresh aspect and considerably greater vesicularity as compared to the latter, the Shona-type volcanics make up the shallower and younger horizons in the basalt stratigraphy. Some of these structural features are crowned with a well-developed cone-shaped superstructure, a likely volcano. This might suggest that Shona-type volcanics are products of within-plate volcanism. Besides, such volcanics have been recovered from the linear rise linking the Spiess and Bouvet volcanoes, in which they are associated with strongly enriched basalts identical to those from the SWIR rift valley.

We have advanced two hypotheses to account for the origin of the Shona Rise volcanics. One draws on the earlier inference of a fluid-rich plume material spreading along the underside of the lithosphere and likely providing a mantle source of enriched melts. In the above discussion, evidence was cited that in mantle-level intermediate magma chambers such melts may have been contaminated with surrounding rocks. Our further inference is that in a compressional setting, involving within-plate stresses, magma chambers become closed systems, with the ensuing dramatic increase in the interaction of melt with chamber walls, composed of a strongly depleted restite. S. G. Skolotnev's geodynamic model [*Skolotnev,* 2000] calls for compressional environments arising periodically in the vicinity of the Bouvet TJ within the South American and Antarctic plates, i.e., where Shona-type volcanics have been encountered. Such environments are equally conceivable in the formation of the Shona Smt., distinguished by its tectonic complexity, with gabbroic rocks occurring at the top of the rise. Assimilation of restite material changed significantly the melt composition. Its plume-related characteristics were considerably suppressed, the melt becoming enriched in Cr and Mg, which are contained in great amounts in the restite. Subsequent magma differentiation in the presence of fluids in a closed chamber, rendering the fluid more strongly oxidized, predetermined a melt evolution following the Bowen trend. Early precipitation of Fe- and Ti-bearing phases gave rise to a volcanic suite resembling calc-alkaline ones. The high Cr abundance is a geochemical feature common to basalts from two distinct volcanic suites encountered jointly on the linear rise between Bouvet and Spiess volcanoes. Apparently, in compliance with the aforesaid, as this rise was in the making,

an extensional regime with a spreading plume material producing enriched melts gave way to a compressional regime with assimilation of lithospheric material and fluid evolution providing major controls on the composition of melts that were forming.

Note also the theoretical possibility of low-Ti orthopyroxene-bearing tholeiitic melts being produced by partial melting in diapirs rising beneath mid-oceanic ridges, as shown in [*Green et al.,* 1979]. According to these workers, this occurs at relatively low-pressure conditions, when a rising diapir that has experienced partial melting undergoes remelting in its further ascent. A tangible example of such a melt is described in [*Danyushevsky et al.,* 1987]. It was detected as a melt inclusion in an olivine grain from Vema Fracture Zone basalts, and it differs from the other oceanic-ridge tholeiites in having extremely low TiO_2, K_2O, and Na_2O and elevated SiO_2 and CaO contents. Hence, if one ignores potassium, this melt composition is to some extent similar to the most primitive basaltic compositions from the Shona Smt. In view of the above, we favor the opinion that melting of the plume material was decisive in the petrogenesis of volcanics such as those from the Shona Smt., although it presumably took place at low-P conditions.

Another hypothesis to account for the genesis of the singular volcanics from the Shona Smt. draws on the geological complexity of the South Atlantic. At the east flank of the MAR at ca. 15°E, an extinct mid-oceanic ridge occurs trending roughly N-S and converging orthogonally to the north with the Falkland-Agulhas Fracture Zone. Judging from the available magnetic anomalies, this ridge was active between Chrons 34 and 27 (100–60 Ma) [*La Brecque and Hayes,* 1979]. Its extinction is attributed to a new, parallel spreading axis appearing a considerable distance westward within the MAR between Chrons 31 and 25 (68–56 Ma).

West of this fossil spreading zone, at the east flank of the MAR between 2° and 10°E, the arcuate Meteor Rise lies. In shape and dimensions, it is quite comparable to the Scotia island arc. It is most likely that this volcanic rise, just like the Scotia arc, is of an island-arc origin. Its genesis may be envisioned as follows. West of the fossil spreading zone, a block of thick consolidated crust (Falkland Plateau) was situated. It obstructed the normal opening of the South Atlantic. Collision of the crust generated west of the MAR paleorift with the thick Falkland Plateau crust gave rise to a subduction zone with its corresponding volcanic (island-arc) rise, Meteor. Subsequently, after a jump in spreading a considerable distance west, this volcanic rise, alongside the MAR paleorift, ceased to exist as an island arc.

Unfortunately, no studies in the composition of the Meteor Rise are known to us thus far. However, the Shona Smt., judging from the volcanic compositions from it, can be viewed as a westernmost segment of a Late Cretaceous island arc, cut by the younger MAR structures.

Discussion

The main factors responsible for the compositional diversity of volcanic rocks in the Bouvet TJ region include (i) mantle plume activity, (ii) intricate geodynamic setup at the triple junction that gave rise to a variety of modes of interaction of plume magmatism and lithospheric material and, (iii) possibly, the regional geological prehistory. The slow spreading rate and ensuing inefficient mixing of the heterogeneous mantle material resulted in strong spatial variations in basaltic compositions.

The deep mantle plume beneath the Bouvet TJ region is rising via two principal channels, whose surface manifestations are the Bouvet and Spiess volcanic edifices. Apparently, these channels are fed at depth from a single source region, roughly ellipsoidal in shape and elongated NW due to the material flowing in this direction. Beneath Bouvet I., the channel is more steep and hot, which results in this area in greater lithospheric thicknesses and long-lived intermediate magma chambers, in which melts undergo a more profound crystal differentiation. The plume heads produce melts enriched in lithophile elements and radiogenic isotopes. The manifestations of plume activity in the region set in no earlier than 2 to 2.5 m.y. BP.

At the Spiess Ridge, the plume is located beneath the spreading axis, which results in its melts mixing with depleted tholeiitic melts. But the interaction of the two mantle sources is not limited to mixing processes, which are in themselves rather complex. Partial melting conditions in these source regions are changing, one possible result being the involvement in melting of a metasomatized mantle, whose fragments may have survived from an early rifting stage. The plume head localized beneath the Spiess Ridge affects the rift volcanism at the nearby MAR as well. In this case, however, the mixing process has a different character. Enriched rock varieties are distributed discretely among the depleted basalts, with depleted source signatures in them predominating over plume source signatures.

Near the Bouvet I., the mantle plume is localized off the spreading axis but, nevertheless, it exerts a considerable influence on the rift volcanism. Firstly, the rift valley is the site of eruption of basalts derived from liquids generated directly through partial melting of the plume material. Secondly, depleted rocks are virtually absent, and prevailing rocks are enriched tholeiites, which are mixing products of depleted and plume-derived melts. The proportion of the plume component in the enriched basalts is large enough.

From these two principal channels, a plume material rich in the fluid phase and elements with a strong affinity for this phase, in particular, K and P, is spreading along the underside of the lithosphere. These fluid-saturated plume derivatives may also produce melts enriched in K, P, etc. Due to their enrichment in fluids, these melts react to their surrounding rocks, apparently, in intermediate magma chambers in the upper mantle. This may result in a non-uniform Cr enrichment of the melts. Eruptions of basalts derived from melts thus formed are observed in lithospheric extension areas both along the plate boundaries such as the Southwest Indian Ridge rift valley and within the plates.

In the case where magma generation zones related to fluid-saturated plume derivatives are formed in compressional settings, further evolution of such a closed igneous system gives rise to closed magma chambers, presumably in the depleted upper mantle, in which extensive assimilation of the wall

rocks and profound differentiation, both processes involving fluids, produce a volcanic suite resembling calc-alkaline ones. Such a process might have taken place in the course of creation of the Shona Smt. as well, but earlier in geological time. Alternatively, the Shona Smt. might be a fragment of an ancient intraoceanic island arc.

In the immediate vicinity of the triple junction, basalts occur anomalously enriched in P and in a number of trace elements (Th, Ba, B, Ce), as well as in radiogenic isotopes. In terms of these parameters and their mode of differentiation, these rocks are sharply dissimilar to the rest of the basalts in the region. The preferable candidate for source material to account for such isotopic fingerprints may be the continental mantle or ancient oceanic crust. In the course of the complex regional geological prehistory, some continental mantle or ancient oceanic crust might have survived in blocks surrounded by a younger oceanic lithosphere. In the vicinity of the Bouvet TJ, these blocks presumably occurred in anomalously hot lithospheric zones, in particular, while the three spreading ridges were converging at a point, and underwent partial melting.

Conclusions

Mafic volcanites from the Bouvet TJ fall into six geochemically distinct groups:

(1) N-MORB, the most widespread type, derived from a depleted mantle source and encountered throughout the study area.

(2) Subalkaline volcanics, hawaiites and mugearites, strongly enriched in lithophile elements and radiogenic isotopes and composing the Bouvet volcanic rise, and compositionally similar basalts and basaltic andesites from the Spiess Ridge, generated in a deeper, fertile mantle region.

(3) Relatively slightly enriched basalts (T-MORB), derived by the mixing of Type 1 and 2 melts and exposed near the axes of the Mid-Atlantic, Southwest Indian, and America-Antarctic ridges.

(4) Basalts with a degree of enrichment in lithophile trace elements similar to the Spiess Ridge and Bouvet I., but higher in K, P, Ti, and Cr. These are developed within extensional structures: the rift valley of the Southwest Indian Ridge, grabens of the East Dislocation Zone, and the linear rise between the Spiess Ridge and Bouvet volcano. Their parental melts presumably separated from a plume material that was spreading from the main channels and underwent differentiation in the mantle in the presence of fluids.

(5) A volcanic suite ranging from basalt to rhyolite, characterized by low concentrations of lithophile elements and particularly of Ti, and exposed on the Shona Seamount and other compressional features within the Antarctic and South American plates near the Bouvet TJ. Unlike the first four types, which display tholeiitic differentiation trends, these rocks are calc-alkaline. Their parental melts were presumably related to a plume material as well, but subsequently they underwent a profound differentiation involving fluids and assimilated surrounding rocks in closed magma chambers in the upper mantle. Alternatively, the Shona Smt. might be a fragment of an ancient oceanic island arc.

(6) Enriched basalts that differ from the other enriched types in having very high P and radiogenic isotope abundances and that compose a tectonic uplift near the junction of the three rifts. Presumably, their primary melt compositions were affected by the melting of blocks composed of materials strongly enriched in radiogenic isotopes (continental mantle? ancient oceanic crust?) in anomalously hot lithospheric regions. Therefore, the main factors responsible for the compositional diversity of volcanic rocks in this region include (i) mantle source heterogeneity, (ii) mantle plume activity, (iii) intricate geodynamic setup at the triple junction giving rise to stresses in adjacent plate areas, and (iv) the regional geological prehistory. The slow spreading rate and ensuing sluggish mixing of the heterogeneous mantle material result in strong spatial variations in basaltic compositions.

Acknowledgments. This study was supported by the RF Ministry of Science and the Russian Foundation for Basic Research (grant no. 97-05-64737).

References

Apotria, T. G., and N. H. Gray, Absolute motion and evolution of the Bouvet triple junction, *Nature, 316,* (6029), 623–625, 1985.

Apotria, T. G., and N. H. Gray, The evolution of the Bouvet triple junction: Implications of its absolute motion, *Tectonophysics, 148,* (3/4), 177–193, 1988.

Cande, S. C., and D. V. Kent, Revised calibration of geomagnetic polarity time scale for the Late Cretaceous and Cenozoic, *J. Geophys. Res., 100,* (B4), 6093–6095, 1995.

Carrara, G., G. Bortoluzzi, N. Zitellini, E. Bonatti, D. Brunelli, A. Cipriani, P. Fabretti, L. Gasperini, M. Ligi, D. Penitenti, F. Sciute, A. Mazarovich, A. Peyve, N. Turko, S. Skolotnev, and D. Gilod, The Bouvet triple junction region (South Atlantic): A report on two geological expeditions, *Giornale di Geologia, 59,* Ser. 3a, (1–2), 19–33, 1997.

Danyushevsky, L., A. Sobolev, and L. Dmitriev, Orthopyroxene-bearing low-Ti tholeiites: A new type of oceanic-rift tholeiites, *Dokl. Akad. Nauk SSSR, 292,* (6), 1449–1453, 1987 (in Russian).

Dick, H. J., R. L. Fisher, and W. B. Bryan, Mineralogic variability of the uppermost mantle along mid-ocean ridges, *Earth Planet. Sci. Lett., 69,* (1), 88–106, 1984.

Dickey, J. S., F. A. Frey, S. R. Hart, and E. B. Watson, Geochemistry and petrology of dredged basalts from the Bouvet triple junction, South Atlantic, *Geoch. Cosmochim., 41,* 1105–1118, 1977.

Didenko A., A. A. Peyve, and L. Tikhonov, Petromagnetic and petrologic variations along the Mid-Atlantic and Southwest Indian ridges at the Bouvet triple junction, *Fiz. Zemli, 12,* 47–66, 1999 (in Russian).

Dubinin E., N. Sushchevskaya, and A. Grokholsky, Evolution of spreading ridges in the South Atlantic and the spatial and temporal position of the Bouvet triple junction, *Russ. J. Earth Sci., 1,* (4), 1999.

Frolova, T., I. Burikova, A. Gushchin, V. Frolov, and V. Syvorotkin, *The Origin of Island-arc Volcanic Suites,* 275 pp., Nedra, Moscow, 1985 (in Russian).

Green, D. H., W. D. Hibberson, and A. L. Jaques, *The Earth: Its Origin, Structure and Evolution,* pp. 265–290, London, Acad. Press, 1979.

Klein, E. M., and Ch. H. Langmuir, Global correlations of ocean ridge basalt chemistry with axial depth and crustal thickness,

J. Geophys. Res., 92, (B8), 8089–8115, 1987.

Kleinrock, M. C., and J. P. Morgan, Triple junction reconstruction, *J. Geophys. Res., 93,* (B4), 2981–2996, 1988.

Kurz, M. D., A. P. Le Roex, and H. Dick, Isotope geochemistry of oceanic mantle near the Bouvet triple junction, *Geoch. Cosmochim, 62,* (5), 841–852, 1998.

LaBrecque, J. L., and D. E. Hayes, Seafloor spreading history of the Agulhas basin, *Earth Planet. Sci. Lett., 45,* 411–428, 1979.

Le Roex, A. P., and A. J. Erlank, Quantitative evaluation of fractional crystallization in Bouvet island lavas, *J. Volcan. Geotherm. Res., 13,* 309–338, 1982.

Le Roex, A. P., H. Dick, A. J. Erlank, A. M. Reid, F. A. Frey, and S. R. Hart, Geochemistry, mineralogy and petrogenesis of lavas erupted along the Southwest Indian Ridge between the Bouvet Triple Junction and 11 Degrees East, *J. Petrol., 24,* (3), 267–318, 1983.

Le Roex, A. P., H. Dick, A. M. Reid, F. A. Frey, and A. J. Erlank, Petrology and geochemistry of basalts from the American-Antarctic Ridge, Southern Ocean: Implications for the westward influence of the Bouvet mantle plume, *Contrib. Mineral. Petrol., 90,* 367–380, 1985.

Le Roex, A. P., H. Dick, L. Gulen, A. M. Reid, and A. J. Erlank, Local and regional heterogeneity in MORB from the Mid-Atlantic Ridge between 54.5 S and 51 S: Evidence for geochemical enrichment, *Geoch. Cosmochim., 51,* 541–555, 1987.

Le Roex, A. P., H. J. B. Dick, and R. T. Watkins, Petrogenesis of anomalous K-enriched MORB from the Southwest Indian ridge: 11° 53′ E to 14°38′ E, *Contrib. Mineral. Petrol., 110,* 253–268, 1992.

Ligi, M., E. Bonatti, G. Bortoluzzi, G. Carrara, P. Fabretti, D. Penitenti, D. Gilod, A. A. Peyve, S. Skolotnev, and N. Turko, Death and transfiguration of a triple junction in the South Atlantic, *Science, 276,* 243–245, 1997.

Ligi, M., E. Bonatti, G. Bortoluzzi, G. Carrara, P. Fabretti, N. Zitellini, D. Gilod, A. Peyve, S. Skolotnev, and N. Turko, Bouvet triple junction in the South Atlantic: Geology and evolution, *J. Geophys. Res., 104,* (B12), 29,365–29,386, 1999.

Mazarovich A., A. A. Peyve, N. Zitellini, A. Perfiliev, Yu. Raznitsyn, N. Turko, V. Simonov, S. Averyanov, A. Bortoluzzi, A. Bulychev, L. Gasperini, D. Gilod, V. Gladun, L. Yevgrafov, V. Yefimov, V. Kolobov, M. Ligi, E. Lodolo, A. Pertsev, S. Yu. Sokolov, and F. Sciute, Morthostructure of the Bouvet Island area, *Dokl. Ross. Akad. Nauk, 342,* (3), 354–357, 1995 (in Russian).

McCulloch, M. T., and J. A. Gamble, Geochemical and geodynamical constraints on subduction zone magmatism, *Earth Planet. Sci. Lett., 102,* 358–374, 1991.

Mitchell, N. C., and R. A. Livermore, Spiess ridge: An axial high on the slow spreading Southwest Indian ridge, *J. Geophys. Res., 103,* (B7), 15,457–15,471, 1998.

Peyve, A. A., A. Perfiliev, Yu. Pushcharovsky, V. Simonov, N. Turko, and Yu. Raznitsyn, The structure of the southern terminus of the Mid-Atlantic Ridge (Bouvet triple junction), *Geotektonika, 1,* 51–68, 1995 (in Russian).

Peyve, A. A., N. Turko, S. Skolotnev, N. Sushchevskaya, M. Ligi, P. Fabretti, A. Mazarovich, S. Yu. Sokolov, and D. A. Gilod, The Bouvet triple junction: Its evolutionary and structural peculiarities, *Tr. Geol. Inst. Ross. Akad. Nauk, 511, in The Issues of Geodynamics of the Lithosphere,* pp. 91–109, Nauka, Moscow, 1999 (in Russian).

Peyve, A. A., N. Zitellini, A. Perfiliev, A. Mazarovich, Yu. Raznitsyn, N. Turko, V. Simonov, S. Averyanov, D. Bortoluzzi, A. Bulychev, L. Gasperini, D. A. Gilod, V. Gladun, L. Yevgrafov, V. Yefimov, et al., The structure of the Mid-Atlantic Ridge at the Bouvet triple junction, *Dokl. Ross. Akad. Nauk, 338,* (5), 645–648, 1994 (in Russian).

Pushcharovsky, Yu., Tectonics and geodynamics of South Atlantic spreading ridges, *Geotectonics, 4,* 286–295, 1998.

Pushcharovsky, Yu., V. Simonov, A. A. Peyve, V. Kolobov, Yu. Tikunov, and M. Melgunov, Correlations of basaltic geochemistry with geodynamic settings at the Bouvet triple junction, South Atlantic, *Dokl. Ross. Akad. Nauk, 361,* (2), 1–4, 1998 (in Russian).

Ringwood, A. E., Slab-mantle interactions 3. Petrogenesis of intraplate magmas and structure of the upper mantle, *Chem. Geol., 82,* 187–207, 1990.

Schilling, J. G., G. Tompson, R. Kingsley, and S. Humphris, Hotspot-migrating ridge interaction in the South Atlantic, *Nature, 313,* (5999), 187–191, 1985.

Sclater, J. G., C. Bowin, R. Hey, H. Haskins, J. Peirce, J. Phillips, and C. Tapscott, The Bouvet triple junction, *J. Geophys. Res., 81,* 1857–1869, 1976.

Seyler, M., and E. Bonatti, Regional-scale interaction in lherzolitic mantle in the Romanche Fracture zone, Atlantic Ocean, *Earth Planet. Sci. Lett., 146,* 273–281, 1997.

Simonov, V. A., A. A. Peyve, V. Yu. Kolobov, A. A. Milosnov, and S. V. Kovyazin, Igneous and hydrothermal processes in the Bouvet triple junction region (South Atlantic), *Terra Nova, 8,* 45–424, 1996.

Simonov, V., A. A. Peyve, V. Kolobov, and Yu. Tikunov, Geochemistry and geodynamic affinity of mafic rocks from the Bouvet triple junction, South Atlantic, *Petrologiya, 8,* (1), 38–52, 2000.

Skolotnev, S., Secondary alterations in basaltic rocks from the Klyuchevskoy cluster of volcanoes, in *Mineralogical Transformations in Oceanic Crustal Rocks,* 241 pp., Nauka, Moscow, 1984 (in Russian).

Skolotnev, S., Structural factors in the geological history of the Bouvet triple junction, South Atlantic, *Geotektonika,* 2000.

Sushchevskaya, N., E. V. Koptev-Dvornikov, N. Migdisova, D. Khvorov, A. A. Peyve, S. Skolotnev, B. Belyatsky, and V. Kamenetsky, Crystallization and geochemistry of tholeiitic melts at the western terminus of the Southwest Indian Ridge (Spiess Ridge) at the Bouvet triple junction, *Russ. J. Earth Sci., 1,* (3), 221–251, 1999.

(Received July 19, 2001)